ASH BED ANALYSIS OF THE CRETACEOUS EAGLE FORD SHALE USING ID TIMS U/PB METHODS: IMPLICATIONS FOR BIOSTRATIGRAPHIC REFINEMENT AND CORRELATIONS WITHIN THE WESTERN INTERIOR SEAWAY

A Thesis

by

MICHAEL JAMES DELUCA

Submitted to the Office of Graduate and Professional Studies of
Texas A&M University
in partial fulfillment of the requirements for the degree of

MASTER OF SCIENCE

Chair of Committee,	Brent V. Miller
Committee Co-Chair,	Michael C. Pope
Committee member,	Debbie J. Thomas
Head of Department,	Michael C. Pope

August 2016

Major Subject: Geology

ABSTRACT

The Cenomanian-Turonian Eagle Ford Group was deposited within the Southern Cretaceous Western Interior Seaway (KWIS) and records the onset and duration of the Oceanic Anoxic Event 2 (OAE2). Lozier Canyon in Val Verde country, Texas provides a unique opportunity to integrate subsurface data and core with a laterally continuous and exposed outcrop section. This study provides U/Pb ID-TIMS (Isotope dilution thermal mass spectrometry) zircon ages for ash beds within the Eagle Ford Group. These high precision age markers are utilized for detailed regional correlations as well as calibration of globally recognizable isotopic events. Astrochronologic age models provide an estimate for the duration of the hiatus observed near the C/T boundary across much of North America, as well as reasonable estimates of significant isotopic events, biostratigrahic datums, and regionally identifiable stratigraphic surfaces. A minimum age constraint of the Buda/Eagle Ford contact is 97.14 ± 0.36 Ma, and a maximum age constraint for the Eagle Ford/Austin contact is 91.23 ± 0.13 Ma. ASM derived rock accumulation rates range from 0.599-0.794 cm/ka for the Lower Eagle Ford and from 0.866-0.876 cm/ka for the Upper Eagle Ford. Integration of bandpass short eccentricity signals, bulk $\delta^{13}C$ isotope data, and zircon age constraint from directly below the C/T unconformity suggests an overall duration of ~0.71 Ma for OAE2, which is similar with other duration estimates of this event throughout the KWIS. This suggests that Lozier Canyon contains a relatively complete OAE2 record, and potentially records the C-T

boundary. Biostratigraphy and $\delta^{13}C$ suggest moderate (10's-100's ky) amount of time missing at the C-T unconformity.

DEDICATION

I would like to dedicate this thesis to my parents, grandparents, and to Maddy for their undying love and support.

ACKNOWLEDGEMENTS

I would first and foremost like to thank Dr. Brent Miller, who gave me the opportunity to attend Texas A&M University and become a part of this research project. His support and guidance throughout my time at Texas A&M has far surpassed that of a typical mentorship, and it has had a profound impact on my life. I would also like to thank my co-chair Dr. Mike Pope and committee member Dr. Debbie Thomas, for their insight and support throughout this project. Their careful review of this work has been invaluable towards its progress.

Additionally, I would like to thank the Berg-Hughes Center for supporting this research. I would also like to thank Dr. Art Donovan and BP for granting access to Lozier Canyon and its datasets. A special thanks to Matthew Wehner and Rand Gardner, who were an invaluable resource for sample collection and collaboration at Lozier Canyon. Thanks to Luz Romero for her technical guidance and support in the lab.

I would like to thank the faculty at Texas A&M for the unbelievable opportunity to see some amazing geology across the country and for the phenomenal education I have received. I would like to specially thank Dr. Tom Olszewski and Dr. Mike Pope for their mentorship throughout the years. Finally, I would like to thank my friends and fellow graduate students, and my office mates Matt Loveley, David Lewis, and Joe Hill for the numerous ways they have supported me throughout my studies at Texas A&M.

TABLE OF CONTENTS

Page

LIST OF FIGURES

Page

LIST OF TABLES

Page

1. INTRODUCTION

The Middle Cretaceous (Cenomanian-Turonian) Eagle Ford Group of Val Verde and Terrell County, Texas consists of interbedded siliciclastic and carbonate strata that records the onset of the global ocean anoxic event (OAE 2) and the Cenomanian-Turonian mass extinction (Denne et al., 2014). Without high-resolution temporal constraints, however, the detailed correlation and time-equivalence of these events with other better-studied sections is poorly constrained and the Texas sections will remain poorly integrated into regional basin- or global-scale understanding of the Middle-Cretaceous. Fortunately, the southwest Texas sections contain numerous volcanic ash deposits that are suitable for ID-TIMS U/Pb zircon dating, which can provide a high-resolution chronostratigraphic framework for these outcrops and a finely correlation with better-studied sections in the Western Interior Seaway (WIS; Fig. 1).

The basal Turonian stage GSSP is defined near Pueblo, Co where it occurs within the Bridge Creek Limestone Member of the Greenhorn Limestone Formation (Gradstein et al., 2012) and is one of the most precisely defined stage-level boundaries in geologic time at 93.9 ± 0.2 Ma (Gradstein et al., 2012). In the 2012 Geologic Time Scale (GTS 2012: Gradstein et al., 2012), the boundary is defined as the lowest occurrence of the Watinoceras devonese ammonite biozone and occurs in the middle of a global positive carbon-13 excursion during an interval of widespread deposition of organic-rich shale, the Oceanic Anoxic Event 2, or "OAE II" (Schlanger and Jenkyns, 2007). Although the exact trigger(s) and timing of this event are poorly understood

(Bond and Wignall, 2014; Turgeon and Creaser, 2008; Jenkyns, 2010), OAE2 is thought to have led to the demise of a variety of molluscs, planktic foraminifera, and nannoplankton (Eldrett et al., 2014; Raup and Sepkoski, 1984). Most of the information about the timing and biostratigraphic effects of OAE2 in North America is from studies in the central to northern segments of the Western Interior Seaway (WIS). The west Texas Eagle Ford outcrops provide a more distal setting, still influenced by similar epeiric sea conditions, but also nearer to open-ocean influences at the southern aperture of the WIS (Corbett et al., 2014). Thus, high-resolution chronostratigraphy coupled with detailed biostratigraphy of the southwest Texas sections can potentially add new information about relationships between, and timing of, paleoenvironmental changes and biotic variability across the basin not recorded in the central WIS sections. For example, the apparent diachroneity of organic-rich sediment deposition and the carbon isotope excursion as seen in other WIS sections, or in European OAE2 sections (Jenkyns, 2010). Anoxic conditions during deposition of the Eagle Ford Group are proposed to have been co-dependent upon sea level and bathymetric restriction of the circulation above the Edwards and Sligo platforms (Donovan et al., 2012).

This study presents high precision zircon ID-TIMS geochronology of the Eagle Ford Group at Lozier Canyon and the surrounding areas to provide a detailed geochronologic framework, refine the Cenomanian-Turonian biostratigraphy and correlations with northern WIS study sites, and to clarify the timing and evolution of basin restriction and transgressive-regressive cycles within the succession. Finally, this study also provides astrochronologic tuning of the Eagle Ford Group at Lozier Canyon.

2. GEOLOGIC BACKGROUND

2.1 The Late Cretaceous Western Interior Seaway

The WIS is part of a north-south oriented foreland basin that developed by flexural subsidence during the Sevier Orogeny, the maximum extent of which reached from Arctic Canada to the Gulf of Mexico (Kauffman, 1977). The Sevier thrust belt was responsible for extensive volcanism throughout the Cretaceous with ash beds of the WIS basin recording over 200 events, some of which can be traced hundreds or thousands of miles although their precise origin and timing is not well understood (Kauffman, 1997; Elder, 1988). During the Middle-Late Cretaceous, the WIS was a shallow, epeiric sea (Corbett and Watkins, 2013). Estimates of the depositional age of the Eagle Ford Group are largely dependent upon biostratigraphic ages and range from late Cenomanian to earliest Coniacian (Denne et al., 2014). The WIS sediments were locally subjected to significant post-depositional alteration by regional tectonism (Kauffman, 1977).

The Eagle Ford Group was deposited near the maximum flooding surface of the 1st-order Zuni sequence of Sloss (1963) and was initiated during transgression over the Central Texas Platform during the Late Cenomanian (Gardner, 2013; Denne et al., 2014). The underlying Comanche Platform formed during the Albian and Early Cenomanian, and affected the physiography of the overlying Eagle Ford Group (Donovan, 2010). The Eagle Ford Group in west Texas is time-equivalent to the prolific mudstone reservoirs of south Texas, and is separated from the distinctive "Eaglebine" (unofficial term for the combined Eagle Ford and Woodbine) deposits of the east Texas

basin by the San Marcos arch (Hentz et al., 2014). The Eaglebine sediments were strongly influenced by Woodbine Delta deposition to the east and are mainly siliciclastic-dominated. West of the San Marcos Arch the Eagle Ford Group is primarily a carbonate system (Hentz et al., 2014). The Eagle Ford Group ranges in thickness from 40 feet on the San Marcos Arch to more than 400 feet in the Maverick basin (Hentz and Ruppel, 2010; Tian and Ayers, 2013). The Eagle Ford Group unconformably overlies the Buda Limestone, and is overlain unconformably by the Austin Chalk; both contacts are regionally correlative surfaces that can be traced across the San Marcos arch (Hentz and Ruppel, 2010).

2.2 Lozier Canyon

In southwest Texas, the Eagle Ford Group outcrops in Lozier Canyon, Antonio Creek, Osman Canyon, and along Tx Hwy 90, providing an opportunity to study a complete vertical section of an unconventional reservoir, as well as easy access to abundant ash beds (Donovan et al., 2012). Many roadside exposures in the region show severe weathering, limited vertical access to the strata, and limited vertical continuity of the stratigraphic section (Donovan et al., 2012). The Eagle Ford Group is an interbedded siliciclastic and carbonate unit that has a distinctive lower unit dominated by dark, organic-rich (up to 5-6% TOC) carbonate-rich shale, and an upper unit consisting of thinly interstratified shale (1-3 %TOC), limestone, and siltstone (Donovan et al., 2012; Dawson, 2000). The units within the Eagle Ford Group have a long and complex history of stratigraphic nomenclature, but for simplification was subdivided into five lithostratigraphic members (A-E), each of which are bound by regionally mappable

unconformities (Donovan et al., 2012). Units A and B constitute the Lower Eagle Ford Formation, and units C, D, and E comprise the Upper Eagle Ford Formation (Donovan et al., 2012). In the Lower Eagle Ford Formation, Unit A consists of wave-stratified foraminiferal grainstone with black mudstone interbeds, and Unit B consists of black mudstone with foraminiferal packstone/grainstone interbeds (Gardner, 2013). Within the Upper Eagle Ford Formation, Unit C consists of bioturbated interbeds of pyrite-rich gray mudstone with light gray foraminiferal packstone beds, Unit D consists of nodular-bedded, bioturbated skeletal wackestone/packstone and mudstone, and Unit E consists of bioturbated wave-stratified grainstone interbedded with mudstone and bentonite beds (Gardner, 2013).

At Lozier Canyon, biostratigraphic studies focused primarily on microfossils, specifically calcareous nannofossils, foraminifera, and palynology with a typical sample interval of two feet (Donovan and Staerker, 2010). The Cenomanian-Turonian (C-T) boundary can be correlated between the Rock Canyon GSSP and Lozier Canyon by comparing stable carbon isotope trends and calcareous nannofossil events (Corbett et al., 2014). The lowest occurrence of Q. gartneri and highest occurrence of H. Chiastia occur near the top of a carbon isotope excursion ~10 ft below the C-T boundary (Unit C-D contact), and the highest occurence of C. kennedyi, R. asper, C. loriei, and A. albanius coincides with the base of the OAE 2 excursion and the contact between the Upper and Lower Eagle Ford Group (Corbett et al., 2014).

Chemostratigraphic and high-resolution lithostratigraphic analyses provide a sequence stratigraphic framework at Lozier Canyon (Fig. 2, Gardner, 2013, Donovan et

al., 2012). This includes a centimeter-scale measured section, lithostratigraphic analyses using polished hand samples and thin sections, and handheld spectral gamma-ray scintillometer profiles (Gardner, 2013). These datasets suggest that the Eagle Ford group within Lozier Canyon and the surrounding region is laterally continuous to the bed level over several miles, with a suggested maximum thickness variation of <7% (Gardner, 2013). The minor variation in thickness and Spectral Gamma-ray (SGR) logs of units A through E at Lozier and Antonio Canyon suggest deposition occurred on a carbonate ramp with little or no slope (Gardner, 2013). Sedimentary structures suggest that the Eagle Ford was primarily deposited above storm wave base, and geochemical and ichnofossil data suggest that the lower A and B units were deposited in anoxic settings, whereas the upper C, D, and E were deposited in dysoxic settings. These lithostratigraphic, biostratigraphic, and chemostratigraphic analyses are used to define chronostratigraphic intervals and boundaries but have serious limitations for regional-scale correlations due to the uncertainty involved in the possibility of time-transgressive units, events, and surfaces.

2.3 ID-TIMS Geochronology

ID-TIMS dating of zircon-bearing volcanic ash deposits throughout the Eagle Ford Group provides a unique opportunity to better constrain stage boundaries within the strata at Lozier Canyon and to correlate with the base of the Turonian stage as defined by the GSSP in Pueblo, Co (Meyers, 2012). The Cenomanian-Turonian boundary is extremely well defined at 93.9 Ma ± 0.2 Ma within the USGS #1 Portland core, where the age is derived by integration of radiometric and astrochronologic data (Meyers,

2012). The C-T boundary is defined in GTS 2012 (Gradstein et al., 2012) by ammonite zonation, however correlation of this datum has inherent limitations because the first occurrence (FO) and last occurrence (LO) levels in different sections may not be time-equivalent across the WIS. Zircon age analysis within these deposits at Lozier may shed light on the degree of regional temporal discordance of biostratigraphic correlations surrounding the C-T boundary. LA-ICP-MS dating lacks the necessary resolution to reliably discern age differences between Eagle Ford Group volcanic ash beds, many of which were deposited within 1 myr or less of each other (Donovan, 2010). Imprecise age calibrations for these ash beds may add confusion and incorrectly reassign biozone age durations within these strata. Even when utilizing high-precision methodologies such as CA-ID-TIMS (Mattinson, 2005), there may still be small degrees of either Pb-loss, inheritance, or incorrect common Pb subtraction which may introduce excess systematic scatter among individual zircon analyses. The exclusion of presumed spurious data points and the method of compiling data points presumed to vary by analytical scatter falling to the individual expertise of the geochronologist.

Recent methodological advances in ID-TIMS dating of zircons permits previously unresolvable temporal constraints with analytical precision reaching ≤0.1% uncertainty on single zircon analyses (Samperton et al., 2015). Enhanced precision of ID-TIMS methods has subsequently revealed heterogeneities within ash bed datasets that previously were unresolvable, allowing for more precise and reproducible age constraints. It has become apparent that many ash beds contain zircons that pre-date the time of eruption, and therefore do not record the actual eruptive/depositional age.

However, recognition of these heterogeneities within datasets also has allowed geochronologists to discriminate non-representative ash bed ages by investigating magma-reservoir characteristics, thereby providing a higher overall precision (Samperton et al., 2015). Other supporting evidence such as cathodoluminescence imaging and trace-element characteristics increasingly are being used to screen zircons selected for analysis (Schmitz, 2001). Recent studies have sought to further understand the magmatic origin of complex zircon systems, and how to best interpret high precision U/Pb data to even better resolve precise eruptive ages (Samperton et al., 2015).

Zircon is a particularly robust geochronometer because it is chemically and physically resistant to isotopic resetting (Davis et al., 2003), and the dual decay of two isotopes of U to two isotopes of Pb allow for two distinct "clocks", which are graphically represented using the Concordia diagram (Wetherill, 1956). Any deviation from Concordia may be the result of xenocrystic inheritance, Pb loss, incorrect assumption of Pb_o, or a combined net effect. For zircons older than ~100Ma, these effects are more readily identified due to higher 206Pb:207Pb and therefore a less steep Concordia slope. For zircons younger than ~100 Ma, Concordia is steeper, making analytical scatter about a concordant age less distinguishable from the effects of Pb loss, xenocrystic inheritance, and incorrect Pb_o. In order to minimize the effect of Pb-loss, Mattinson (2005) developed the chemical abrasion method to greatly minimize the inclusion of susceptible outer portions of zircon grains. Despite these advances, the ^{235}U-^{207}Pb clock remains poorly resolved at Cretaceous and younger ages. As a result many high-precision geochronology studies disregard this chronometer and base their age

interpretations on ^{238}U- ^{206}Pb ages. Even if the CA method fully removes the effects of Pb-loss, both systems may show systematic offsets due to inaccurate assumptions in the compositions of common Pb (blank and/or initial). An incorrect common Pb composition will produce a systematic shift in the 235/207 age to a greater degree than the 238/206 age, resulting in mainly lateral shifts on a conventional concordia diagram. To account for this, final age interpretations either are based upon concordia ages or regression intercept ages. Regression intercept ages typically are utilized to distinguish pre-Pb loss ages, recrystallization ages, or both. However, given the asymmetric and lateral dispersion of ages in some datasets herein (high 207/235:206/238 ratios) we attribute this to variations in the Pb_o composition and incorrect assumptions of the Pb_c isotopic composition. We utilize the regression intercept age to quantitatively account for overall variability. This method allows for a clearer graphical representation of the effects of different sources of discordance, with the goal of a more reliable means of interpreting our data arrays. Because each ash bed sample has its own unique set of data characteristics, the age of each ash bed is evaluated by the best method for interpreting the data array of that ash bed.

3. METHODS

3.1 ID-TIMS

Volcanic ash bed samples were collected from the Lozier Canyon/Antonio Creek study site, with care taken to obtain samples with only minimal observable diagenetic alteration. Large fragments were reduced to gravel size using the Badger Jaw Crusher and then disaggregated in the Bico disc pulverizer, to 2 mm or less fragments. For relatively unlithified samples, repeated rinsing with water or dilute HCl or HNO3 was utilized to remove clays or organics, eliminating the need for crushing and pulverizing. The samples were sieved using 125 µm, 355 µm, and 500 µm sieves for four size fractions: <125 µm, 125-355 µm, and > 355 µm. 125-355 µm fractions were processed for zircons, while other samples were sealed and stored. Samples were washed and sonicated for fifteen minutes, and then dried in an oven. Grains were liberated from heavily lithified and/or diagentically altered ash beds by treatment with dilute HCl, HNO3, and HF. Heavy-liquid separations were performed in order to obtain sanidine and zircon density fractions using LVP with a density of 2.55. Zircons were then picked and placed into crucibles and allowed to anneal for 99 hours at 900°C. After annealing, zircons were photographed and selected under plane light based on optical clarity, lack of inclusions, and minimal fractures or cracking. Cathodoluminescence imaging was utilized for several samples to ensure zircons selected for analysis were devoid of xenocrystic cores. Chosen zircons were annealed in the range of 800-1100 °C for 48 hrs and chemically abraded following Mattinson (2005). Final dissolution and

spike equilibration was conducted using HF and HNO_3 in 200 µl Teflon microcap capsule, with a total of 18 samples placed into a Parr-type high-pressure dissolution vessel and heated at 210 °C for 72 hours or more. An internally calibrated, mixed 205Pb-233U-235U spike is used for U-Pb analysis, and is calibrated in reference to two external spike calibration solutions and the EarthTime nominal 100 Ma, 500 Ma, and 2 Ga interlaboratory standards.

Following dissolution, sample solutions were loaded onto Teflon microcolumns with ElChrom® anion resin, which aims to initially wash Zr, Hf, and REE, and then segregate Pb and U by using HCl. U and Pb were loaded on degassed Re filaments using 1µl of silicic acid loading solution. All measurements were conducted on a ThermoFisher™ Triton thermal-ionization mass spectrometer. "YourLab" algorithms of (Schmitz & Schoene, 2007; Schoene et al., 2006) are used for data reduction and IsoPlot 3.00 (Ludwig, 1991) is used for plotting concordia diagrams. Best age interpretations are reported in the form X ± Y (Z) Ma, where X is the mean of the best-age interpretation, Y is the 2-sigma error including systematic error in decay constants, and Y is the 2-sigma error excluding uncertainty in the decay constant. The former error should be used when comparing ages from different methods (Ar/Ar or absolute astrochronology) and the latter for comparisons with U-Pb ages or relative astrochronology (e.g., Schoene et al, 2006).

3.2 Cyclostratigraphy

Datasets for cyclostratigraphic analyses were generated by two methods, the first of which is based on relatively low order facies cyclicity (Fig. 3). Gardner et al, 2013

provide centimeter-scale lithostratigraphy for Lozier Canyon and Antonio Creek; facies were assigned values 1 through 6 and are ordered from high to low in terms of relative interpreted depositional energy. Therefore, the values are assigned the following facies: 1-stratified foraminiferal grainstone, 2-foraminiferal packstone, 3-foram/skeletal wackestone, 4-medium gray shale, 5-dark gray shale, 6-very dark/black shale. These values were plotted against depth with a sampling interval of ~3.81 cm. Cycles were then delineated from dated ash beds to major stratigraphic surfaces. Cycles were defined as a change in lithology irrespective of frequency or amplitude, and were counted from trough to trough. Total time duration possibilities were derived by assuming individual cycles are either the dominant precession (23 ka) or obliquity (41 ka) frequencies. Eccentricity was excluded from analysis because the low frequencies (100 ky and 405 ky cycles) require a higher resolution and a longer record than is provided by this method. This cycle-counting method was applied in both up-section and down-section directions from dated ash beds to compare cyclicity stability. This method was pursued because of the highly detailed cm-scale analysis of Gardner (2013) which integrated petrographic thin section analysis, outcrop Gigapan photography, hand-held gamma-ray scintillometer, and hand sample/outcrop based petrography. Although other datasets such as grayscale are preferred due to higher potential resolution, this dataset provides a unique opportunity to compare interpreted facies changes with grayscale to determine whether grayscale is strictly correlated with overall % CaCO3, facies changes, and Milankovitch-scale cyclicity throughout the Eagle Ford Group. Sampling frequency of Gardner (2013) is roughly 3 cm, and given current ASM results outlined below we

believe that with this sampling interval should be able to identify the lowest frequencies, P1 and P2 terms, which range from 20-25 cm in total period length. However, this method is highly subject to missing beats of cyclicity, which is why obliquity and precession are simultaneously plotted to develop an estimate of the range of possible time durations between anchored ash beds.

.3.3 Astrochronology

Grayscale data was derived from color photos of the BP Lozier Canyon #1 drill core (generously provided by BP), from directly behind the outcrop wall at Lozier Canyon. The core photo width was uniformly cropped to 24.4 mm to avoid irregular sides of core and to decrease the likelihood of including cracks. Cracks and bentonite beds were not removed from the dataset prior to analysis. The color photos were converted to grayscale using Adobe Photoshop's "lab color mode" by isolating and converting the lightness channel to grayscale. Grayscale values were converted to numerical form using ImageJ software and range from 0 (white) to 255 (black). This dataset was then subjected to time-series analysis "Astrochron", which is a package developed for R software (Meyers, 2014). Astrochron requires that all data be in metric format and depth adjusted for a continuous and uniformly sampled record, and therefore all astrochronologic depths are reported in adjusted depths. This dataset spans from the Buda Formation-Eagle Ford Group contact to the Eagle Ford Group-Austin Chalk Formation contact, however due to significant core loss above 162 feet, the 162-190 foot section was not included in the astrochronologic analysis. Evolutive harmonic analysis (EHA) and evolutive power spectral analysis (EPSA) were implemented using three 2π

DPSS tapers and a 6 m moving window. Windows selected for MTM (multi-taper method) analysis include 0-5.18 m, 5.18- 15 m, and 15-27 m for the lower Eagle Ford, and 27-28 m, and 38-49 m for the upper Eagle Ford. These windows were selected between well-known unconformities, which sub-divide them into lithologically related packages. MTM was applied to these windows to obtain candidate frequencies for ASM (average spectral misfit) testing. For this study, F-Test significance level of peaks was set at >85% confidence, and candidates fitting these criteria were utilized for ASM testing. Orbital target periods were derived from Laskar et al. (2004, 2011) and Eldrett et al. (2015) for which the 94-98 Ma Laskar solution was utilized for the Lower Eagle Ford and the 91-94.5 Laskar solution was utilized for the Upper Eagle Ford (Tables S1 and S2;Laskar 2004, 2011; Eldrett et al., 2015) . ASM testing was conducted using 100,000 Monte Carlo simulated spectra with 100 sediment accumulation rates evaluated yielding a critical null hypothesis significance level of <1%. Identified frequencies were subsequently applied to the de-trended and de-meaned grayscale data by bandpass filtering, which reveals the preserved orbital signals within the succession.

4. RESULTS

4.1 U-Pb Dating

Fifteen ash beds were collected from Lozier and Osman Canyon, of which ten yielded zircons. Ash bed sample locations are reported as feet above the Buda Formation/Eagle Ford Group contact. Ash beds sampled for this study span from 1.5 to 177 feet above the Buda limestone; the total stratigraphic thickness at this location is ~180 feet (Table 1). Due to lack of access at Lozier Canyon, the uppermost three ash beds, 155, 170, and 177, were collected from Osman Canyon which is ~ 9 miles east of samples 1.5-135, collected from Lozier Canyon and Antonio Creek. Bed-scale lateral continuity between Lozier Canyon and Antonio Creek is estimated to be no more than 7.3% in unit A, 0.7% in Unit B, 0% in unit C,4.8 % in unit D, and 3.7 % in unit E (Gardner et al., 2013). They attribute low degree of variability between sections to deposition on a carbonate ramp with little or no depositional slope. Although a similar high-resolution lateral continuity study was not conducted between Lozier and Osman Canyon, the unit D/E contact is well preserved at Osman Canyon and ash bed depths are based upon depth above or below that boundary relative to the Lozier measured section. This correlation is considered precise due to the apparently relative synchronous nature of the D/E boundary over this distance and the relatively consistent regional thickness of Eagle Ford units within the study region (Gardner, 2013). Zircon analyses utilized for age interpretation are presented in Table 2.

At Lozier Canyon, 1.5 is the stratigraphically lowest ash bed within the Eagle Ford suitable for sampling; sample 1.5 is 1 inch thick, well lithified, and gray to dark gray (note: all sample numbers correspond to feet above Buda Formation contact). Sample 1.5's mineralogy includes abundant Fe-oxides, clay minerals, and rhombohedral milky-white barite crystals. Zircon crystals are small (5-25 microns longest dimension) and relatively uncommon compared to other ash beds. Grains are elongate prismatic and predominantly clear. In cathodoluminescence images (Fig. 4) grains characteristically reveal little to no internal zonation and generally lack any obvious cores. Fifteen single grains of zircons were selected for analysis, of which eight formed coherent trend on concordia (Fig. 5). Analyses excluded from the final age interpretation were inferred to be xenocrysts or unusably discordant due to Pb loss or incorrect $Pb_{c,}$ correction. The Concordia age of the remaining eight analyses is taken to be the most robust age interpretation because all analyses are concordant and overlap within error. Ash bed 1.5 yields a Concordia age of 97.14 ±0.36 (0.41) Ma, with a MSWD of 5.9.

Ash bed 64.5 is 1-2 inches thick and white-pale yellow. Mineralogy of sample 64.5 is primarily clays and calcite, with minor Fe oxides and feldspar. SEM analysis of several feldspar crystals indicates the presence of rare orthoclase and sanidine grains, which are severely diagenetically altered. Zircons are abundant and are variable in morphology, including small sub-rounded grains, acicular and elongate euhedral grains, and prismatic elongate grains with low c:width ratios. Cathodoluminescence imaging reveals internal zoning and/or core-rim structures (Fig. 6) in many zircons, and tends to be most common within low c:width ratio zircons and least common in elongate and

acicular grains. Twenty-two single zircons and one two-grain aliquot were selected for analysis, of which nine do not yield meaningful results and were rejected. The remaining 13 analyses yield a complex array of ages that can be sub-divided into two coherent suites, of which both appear to have complex and variable ranges in common lead compositions (Fig. 7). The older suite yields regression age of 96.57± 0.13 (0.16) Ma, MSWD 0.56 while the younger suite yields regression age of 95.79±0.24 (0.26) Ma, MSWD 1.2. Relatively low MSWD values for each regression age confirms two distinctive datasets, thereby validating segregation of the two groups. Furthermore, the younger suite age (95.79±0.24 Ma) is the most robust age interpretation for this ash bed because more scatter would be expected if the U-Pb ages were affected by Pb loss (downward shift in concordia ages). More likely is the incorporation of a coherent xenocrystic component in the older age suite.

Ash bed 80 is 1 inch thick, gray to red, and poorly lithified. Mineralogy of ash bed 80 includes Fe oxides, clays, with minor calcite cement. Zircons are relatively uncommon, and range in size from 20-40 microns and are clear to honey-colored. Zircon morphologies within 80 are predominantly euhedral elongate prismatic to elongate acicular, and many contain inclusions that are visible under binocular plane light. 13 single zircon grains were selected for analysis, of which 5 were excluded from final age interpretation. The concordia age of the remaining 8 analyses was taken as the most robust age interpretation, due to the minimization of obvious Pb loss, xenocrystic inheritance, or incorrect common Pb composition (Fig. 8). Ash bed 80 yields a concordia age of 95.23±0.16 (0.22) Ma, MSWD 0.0059.

Ash bed 135 is 0.5 inches thick, and is light brown, slightly unconsolidated and weathered. Overall composition includes kaolinite, calcite, abundant apatite, and minor Fe-oxides. SEM analysis indicates rare sanidine and orthoclase grains in sample 135 that are severely altered. Zircons are scarce, and are mostly elongate prismatic and clear with a size range of 10-20 microns. Of the 13 single grain zircon analyses, 10 were utilized for the final age interpretation. These 10 analyses yield a complex array of data, many of which have higher associated uncertainty largely due to relatively low Pb^{*}:Pb_{c}. This scatter is likely due to inheritance from multiple xenocrystic components (Fig. 9). The youngest four analyses are tightly clustered and concordant, suggesting that these represent the primary eruption date and Pb loss is not the primary cause for scatter within the dataset. Therefore, the concordia age of the youngest 4 grains is used for final age interpretation, and yields 94.65 ± 0.38 (0.42) Ma, MSWD 6.3.

Ash bed 155 is light brown to yellow, moderately lithified with abundant calcite and dolomite. SEM analysis suggest the dominant clay species is kaolinite, and this sample contains rare sanidine grains. Zircons are extremely abundant and mostly elongate and acicular to prismatic. Grains range in size from 20- 40 microns and are clear to pale orange with rare inclusions. Of the 12 single grain zircon analyses, ten were utilized for the final age interpretation. Although analyses are precise and relatively tightly clustered, there is significant systematic scatter, probably associated with initial common Pb correction (Fig. 10). Therefore, the regression age which yields 91.48±0.15 (0.18) Ma, MSWD 1.7 for ash bed 155 is its most robust age interpretation.

Ash bed 177 is 2-3 inches thick, beige to orange and is well lithified with abundant clay and calcite. Zircons are common and are sub-rounded to anhedral and prismatic, ranging in size from 10-25 microns and are clear to pale orange. Of the 18 single zircon grain analyses, 11 were utilized for its age determination. Although all data points are concordant, there is significant scatter in ages, likely due to the common Pb composition (Fig. 11). The regression age is interpreted to be the most robust age, which yields 91.23 ± 0.13 (0.16) Ma, MSWD 1.4.

4.2 Sedimentation Rate Analysis

A first-pass estimate of sedimentation rates was determined by linearly interpolating age against time for intervals between ash beds, not considering total uncertainty on ash bed ages. Sedimentation rates for corresponding intervals calculated in this way are given in Table 3. Further refinement of sedimentation rate is constrained by average spectral misfit (ASM; Meyers and Hinnov,2010; Meyers et al., 2012a; Ma et al., 2014). ASM analysis is largely guided by these parameters, but infers the most statistically relevant sedimentation rate given identified lithological frequencies within a given interval. Additionally, although ASM analyses relies on ash bed interpolated sedimentation rates it is important to note that the windows for each method are not equivalent. For example, the ash bed window from sample 1.5 to 64.5 contains two complete, and a portion of a third, astrochronology windows. This is because windows selected for astrochronology are largely dependent upon lithologic and spatial limitations, irrespective of ash bed location.

4.3 Cyclostratigraphy

Lithologic cyclicity analysis is a further refinement that attempts to honor all available data by determining maximum and minimum sedimentation rates. Rates are constrained by cycle-counting of lithological variations between dated ash beds and assigning time based on astronomical periods for obliquity and precession (41 and 23 ka, respectively). These two astronomical signals should be pervasive throughout the section (guided by our astrochronolgical analysis) and identifiable at the sampling resolution (~3cm) provided by the Gardner et al. (2013) section. These maximum and minimum rates are produced by counting the number of cycles between dated ash beds and major unit boundaries and then by assuming each cycle is related to obliquity, or conversely that each cycle is related to precession. Sedimentation rates calculated through this method are almost certainly underestimated because of small-scale unconformities. The ranges of sedimentation rates using these two astronomic frequencies and the number of cycles per stratigraphic interval are shown in Figure 3.

In figure 3, the colored arrows represent interpolated rock accumulation rates and shaded polygons represent the range of possible rock accumulation rates. Interpolated cyclicity conducted top-down (blue arrows) do not yield sensible results, other than the section from ash bed 64.5 to the A/B contact. This is likely due to interpolation across unidentified unconformities, interference of one or more periodicities (likely), or slight misinterpretation in geochronologic data. Results are often incongruent between top down and bottom up analyses because each section spans a unique zone for analysis. For example, when considering the top-down section from 155 to the C/D boundary,

there is not an equivalent section for the bottom up series. Additionally, between the Eagle Ford/Buda base to the C/D boundary, there are three bottom up sections but only two top down sections. This is because this method is entirely limited by anchoring time at a dated ash bed, and then interpolating to a significant boundary or unconformity. Although this method has the potential to yield non-representative results, these results are easily identified and rejected when compared to zircon age constraint. However, interpolated cyclicity conducted bottom-up yields more reasonable results, suggesting strong obliquity and precession signals are stable within the lower Eagle Ford Group. The validity of the bottom-up (red) interpolation is not compromised by the lack of significant results from the top-down(blue) section because they are comprised of entirely different segments, and are not mirror images of one another. Sedimentation rates derived from this method are presented in tables 4 and 5.

4.4 Astrochronology

Average spectral misfit quantitatively applies spatial cycles of Laskar 2004, 2001 to determine optimal sedimentation rates, while utilizing Monte Carlo simulation to reject the null hypothesis (Eldrett et al., 2015; Meyers and Hinnov.2010; Meyers et al., 2012, Ma et al., 2014). Thus, ASM identifies the optimal sedimentation rate for a given window as a function of time allowing a finer-scale sedimentation rate can be determined by linear extrapolation between U/Pb dated ash beds. The ranges input into ASM testing are 0.5-2 cm/kyr for the lower Eagle Ford Group and 0.2-2 cm/kyr for the upper Eagle Ford Group. Considering these sedimentation rate ranges, the largest frequency tested for ASM analysis in the Lower Eagle Ford is 10 cycles/m, and 6.5

cycles/m for the Upper Eagle Ford. The ASM results are listed in Table 6. Grayscale data was subdivided into packages as follows: 0-5.185m, 5.1816-15m, 15-27m, 27-38m, and 38-49 m. These windows were placed in between widely recognized regional unconformities (major unit boundaries at Lozier), which also bundles these units into lithologically related packages. Frequencies selected for bandpass are compiled into Table 7. Additionally, bandpass signals were derived from the grayscale dataset for each orbital target (Fig. 12). A suitable E1 candidate peak could not be identified in 27-38, and therefore E1 was bandpassed at the plausible range of frequencies as bracketed by the identified E2,E3 frequencies. Orbital frequencies identified by ASM analysis are traced and labelled on EHA and EPSA results (Fig. 13). The E1 bandassed signal is utilized for age model construction, however O1 and E1 EHA tracing yield similar results (Fig. 14).

5. DISCUSSION

U/Pb zircon ages from bentonite beds throughout Lozier Canyon are compared with those at approximately coeval bentonites throughout the WIS dated by similar methods (Fig. 14), and are tied with regional biostratigraphy. Ash beds at Lozier Canyon span a relatively complete record of deposition throughout the sequence, allowing suitable benchmarks for building a geochronologic framework. This pattern is not continuous immediately above the C-T boundary where bioturbation has destroyed original bedding planes. Additionally, the C-T boundary unconformity across much of the KWIS appears to be longer in duration at Lozier Canyon than other sections to the east (Eldrett et al, 2015) or northwest (Meyers, 2012), which here appears to be ~2.61 Mya in duration. This is likely a result of the elevated inherited bathymetry on the drowned Comanche platform in the area of the Lozier Canyon section.

5.1 Regional Ash Bed Markers

The use of regional marker beds that are well characterized and radiometrically dated throughout the WIS have proven to be essential to regional well log interpretations, stratigraphy, and biostratigraphy (Elder, 1988). It is likely that their ash bed "x" is sample 64.5 in Lozier due to stratigraphic position as well as the zircon derived age that is within error of other regional datasets of the deposit (Eldrett et al, 2015). It is unclear whether their ash beds "A" and "B" are preserved at Lozier Canyon, as zircons were not recoverable from candidate ash beds for A or B at Lozier. However, these ash beds may occur at Lozier Canyon and are zircon-poor in this region or are too

thin to be sampled or observed in outcrop. Additional future geochemical and isotopic data may be able to distinguish these ash beds and provide regionally correlatable benchmarks at Lozier Canyon. Identification and sampling of these ash beds may be achieved in the future within the Lozier research core under UV light or XRF microanalyzer. Ash bed 135 (this study) is a likely candidate for regional ash bed "C", however further geochemical analysis is needed to reliably trace candidate ash beds with ages that lie within uncertainty of one another. Ash bed D is likely not preserved at Lozier Canyon, where the C-T unconformity is longer than in other WIS sections.

5.2 Inter-comparison of WIS Geochronology

Increasingly precise resolution via U/Pb ID-TIMS methods has allowed identification of sources of uncertainty and can be identified and addressed within datasets (Bowring and Schmitz, 2003). Thus, the level of precision at which genuine geologic scatter is resolvable from analytical error and other random sources of uncertainty has steadily decreased, opening new avenues of research. Nevertheless, where the geochronologic resolution required approaches this limit, some operator bias is unavoidable. Age constraints from previous work across the basin (Eldrett et al., 2015) appears to be systematically younger than the ages reported here from Lozier Canyon (Fig. 14). Clearly, these discrepancies have significance for the WIS, including regional correlations, calculating rock accumulation rates, astrochronologic tuning, as well as the timing and duration of isotopic events. Ar/Ar dates typically are systematically younger than zircon datasets because incorporation of some component of xenocrystic inheritance, Pb loss, magma residence time, a systematic bias in one of the

decay constants, or the Ar/Ca branching ratio (Schoene, 2006). However, the increasingly popular interpretation that the youngest grain or youngest coherent cluster of grains in a zircon data suite is necessarily the best age estimate must be strongly supported by other criterion within the dataset (Samperton, 2015). This is particularly pronounced within samples that are younger than ~100 Ma, due to the fact that graphical and statistical recognition of Pb-loss grains is difficult due to the "steep" nature of Concordia at a young age. The approach taken here is to make no prior assumptions about the nature of the data and to base the age of each ash bed on what is here considered to be the best interpretation of each data array. While this may introduce an operator bias, it avoids the pitfall of incorrectly forcing on all samples the same causal mechanisms for data point scatter, which there is no a priori reason to assume should have the same causes of data point scatter. For example, ash bed 135 is taken as the concordia age of the youngest 4 analyses (figure 8). This is supported by tight clustering on concordia of these four youngest grains which suggests no Pb loss occurred, and characteristically scattered xenocrystic ages above on concordia. This final age interpretation is verified by cross examination of extracted sedimentation rates, astrochronolgic tuning, and bulk carbon isotope curve (Figs. 9, 15).

5.3 Lozier Canyon Age Constraint

Our work includes one of the stratigraphically lowest ash beds dated within the Eagle Ford to date, which provides a robust benchmark for tracing the timing of transgression throughout the basin, as well as how bathymetry of the underlying Sligo/Edwards margin may have affected the onset of Eagle Ford deposition.

Additionally, the maximum age of the Eagle Ford at Lozier Canyon was not well known, and was thought to be lower Cenomanian based on sparse nannofossil biostratgraphy (Corbett et al., 2014). The LO of C. kennedyi should mark the base of the Lower Cenomanian, however this datum is found relatively high within Lozier Canyon, which was previously assigned to preservational bias (Corbett et al., 2014). Ash bed 1.5 was dated as 97.14 ± 0.36 Ma placing it within the Middle-Late Cenomanian, which brings the utility of this ammonite zonation as a regional time marker into question. Additionally, this ash bed was identified and correlated regionally in outcrops throughout the area, where it generally occurs higher in the section, commonly several feet above the Buda-Eagle Ford contact. Future work in correlating this ash bed across the region may provide insight into the diachronous nature of the onset of Eagle Ford sedimentation. Accurately tracing this ash bed regionally also may provide insight into the origin of the Buda-Eagle Ford Contact karsting, which was suggested to be either exposure-related or meteoric (Eldrett et al., 2015). This may determine the degree of influence paleobathymetry had during the onset of Eagle Ford Group deposition.

5.4 Duration of OAE 2 and the C-T Unconformity at Lozier Canyon

Without precise age constraints the duration of OAE2 is difficult to discern at Lozier Canyon by biostratigraphy and $\delta^{13}C$ data alone. Ash bed 135 is located just beneath the C-T unconformity and is dated at 94.65 ±0.38 Ma. This suggests that Lozier Canyon misses at least the beginning of OAE2 which begins at ~94.7Ma (Eldrett et al., 2015). However, bulk $\delta^{13}C$ data from Lozier Canyon reveal that much of the isotope excursion is recorded at Lozier Canyon. Additionally, astrochronologic tuning between

the Pueblo, CO core and Iona-1 (Eldrett et al., 2015) trace 5-6 short eccentricity (96-127 ky) cycles within the isotope excursion. The Lozier Canyon data records this same orbital signal, for a similar duration (~6 E2, E3 cycles) within the carbon isotope excursion (Fig. 15). The discrepancy can be explained because sample 135 contains xenocrystic components (Fig. 9), and it is possible that some xenocrystic grains were incorporated into the final age interpretation, skewing the final interpretation to an anomalously old age. If the single youngest grain is considered as the most robust age interpretation, sample 135 is 93.10± 1.034 Ma. Although error on this single analysis is relatively high, if we consider the next youngest single grain, 135 is 94.30± 0.496 Ma, and does not greatly change the interpretation. This places 135 within error of the C-T boundary. Considering that ash bed 135 is the most highly variable in the Lozier Canyon dataset, and that we have astrochronologically identified a similar short eccentricity signal and duration at Lozier Canyon, this suggests that Lozier Canyon contains a relatively complete record of OAE2 and perhaps the C-T boundary. The relatively synchronous duration of OAE2 at Lozier Canyon and Iona-1 suggests that local bathymetric and environmental conditions do not affect the onset or duration of anoxic conditions.

If the C-T boundary itself is missing, it can only be missing one half of a short eccentricity cycle (~60ka), otherwise fewer than 6 cycles would be recorded at Lozier Canyon. This requires that the majority time lost during the unconformity took place after the C-T boundary. Although we did not recover ash beds from directly above the unconformity, we infer a disconformity duration of ~2.61 Mya based on interpolating the

astrochronologically derived E1 age mode, and ash beds 155 and 177. Ash bed 80 (95.23±0.22), although ~20 feet lower than the onset of OAE2, allows an extreme maximum estimate of onset OAE2 at Lozier Canyon to between 95.23 Ma to 93.10 Ma. Depending on the method of age interpretation for ash bed 135, OAE2 is either 0.35 Ma (using youngest 4 ages) or 0.7 Ma at Lozier (second youngest age). Eldrett et al. (2015) inferred a duration of 0.71 ±.17 Ma. The Lozier Canyon analysis presented here indicates OAE 2 occurred from 95 to 94.3 Ma, whereas Eldrett et al. estimate is duration from 94.7 to 94.155 Ma.

5.5 Sedimentation Rate Analysis

ASM derived rock accumulation rates for Lozier Canyon imply that sedimentation rates were relatively stable throughout deposition of Eagle Ford strata within ~.1cm/kyr, ranging from 0.599-0.876 cm/kyr. The average rock accumulation rate for the lower Eagle Ford at Lozier Canyon is 0.682 cm/kyr, and 0.871 cm/kyr for the Upper Eagle Ford. This compares to the Iona core sedimentation rates of 1.77 cm/kyr for the Lower Eagle Ford and 1.42 cm/kyr for the Upper Eagle Ford (Eldrett et al., 2015). This implies that the rate of rock accumulation was 38.4% faster at Iona for the Lower Eagle Ford and 61.3% faster for the Upper Eagle Ford.

Considering that Lozier Canyon was deposited in a more proximal setting on the platform, while Iona was deposited in a more distal setting, we can examine the relationship of sediment flux across the basin profile throughout deposition. The ratio of highstand (HST) to transgressive systems tracts (TST) is 3:2 in the Lower Eagle Ford, and 1:3 in the Upper Eagle Ford (Donovan, 2012). It is possible that the Lower Eagle

Ford sedimentation rate is less variable across the slope because paleobathymetric constraints are less limiting at Lozier during HST's than TST's.

6. CONCLUSIONS

High precision ID-TIMS U/Pb ages, as well as astrochronologic tuning of the Eagle Ford Group at Lozier Canyon provides new age constraints on the temporal record of OAE2 and the evolution of depositional environments within the KWIS. Ash bed 1.5 (97.14 ±.36 Ma) provides a minimum age constraint for the onset of deposition of the Eagle Ford above the regionally identifiable K63 sequence boundary. Total rock accumulation between the K63 sequence boundary and this ash bed is regionally variable, and may be due to diachronous transgression, Buda karsting, variable paleobathymetry or some combination of these effects. Future work should aim to characterize and correlate this ash bed with other geochemical methods, such as LA-ICPMS REE or XRF to reliably and consistently distinguish this ash bed marker regionally. This will enable a high-resolution understanding of the duration and variability of transgression over the Buda Limestone.

Rock accumulation rates of the Eagle Ford at Lozier Canyon are significantly lower than other sections in the KWIS for which high-precision data are available, which is reasonable considering the relatively decreased thickness of the Eagle Ford at Lozier Canyon. ASM derived rock accumulation rates suggest rates of 0.599-0.794 cm/ka for the lower Eagle Ford, and 0.866-0.876 cm/ka for the Upper Eagle Ford, and are relatively consistent to within ~.1 cm/ka throughout the section. Rock accumulation rates are up to 38% larger in the Iona-1 core (Eldrett,2015) for the Lower Eagle Ford, and 61% larger in the Upper Eagle Ford. This comparison of precise ASM-derived rock

accumulation rates may suggest an increase in accommodation space, sedimentation rate, or both for the more distal portions of the basin during Upper Eagle Ford deposition relative to the Lower Eagle Ford.

Bulk $\delta^{13}C$ isotope data suggests that the onset of the positive isotope excursion associated with OAE 2 is from 95.01 Ma (Astrochronologic age model derived) to the C/T boundary unconformity 94.65 ± 0.38 Ma (zircon age). We recognize a similar number of short eccentricity cycles within the isotope excursion (~6 full cycles), however the time duration derived from this analysis is insufficient to explain preservation of all six of these correlative cycles.

Ash bed 135 represents one of the most analyzed, yet complex, datasets within this study. Zircons from this ash bed appear to have incorporated one or more xenocrystic components, and therefore final age interpretation is the least robust of this study. The concordia age of the youngest 4 grains form the most coherent cluster, however astrochronologic analysis suggests that this age is too old and only the ages of the two youngest grains are consistent with cyclostratigraphic analysis. Taken this way, the duration of OAE2 at Lozier Canyon spans from ~95.0 to 94.3 Ma, with a duration of ~0.7 Ma. This is reasonable, given the presence of roughly six preserved short eccentricity cycles within the isotopic signature of OAE2. Furthermore, this indicates that Lozier Canyon likely preserves most of OAE2, and possibly the C-T boundary. If the C-T boundary is missing, it is within one short eccentricity cycle (127 ka). This is further supported by the E1 astrochronologic age model which is supplemented by ash beds 155 and 177, suggesting that the majority of time missing within the unconformity

takes place after the C-T boundary. Further studies should seek to identify the most robust age interpretation of ash bed 135, using cathodoluminescence, LA-ICPMS trace element, and XRF characterization in order to fully understand the xenocrystic components within this sample and attempt to more fully constrain the age.

Rock accumulation rates are highest above the C-T boundary (0.866-0.876 cm/ka), and ash beds 155 and 177 provide important constraints on the Eagle Ford-Austin transition. Ash bed 177 lies three feet below the Eagle Ford/Austin contact, and provides a maximum deposition age of the Austin Chalk as 91.23 ±0.13 Ma. Future work should aim to compile zircon ages from the Austin Chalk to compare rock accumulation rate change, as well as precise identification of the T-C boundary which almost certainly lies in the Austin Chalk, and not the Eagle Ford Group at Lozier Canyon.

REFERENCES

Blakey, R., 2014, Colorado Plateau Geosystems. Inc., Western Interior Seaway Series: http://www. cpgeosystems. com/paleomaps. html (accessed August 2014).

Bond, D.P., and Wignall, P.B., 2014, Large igneous provinces and mass extinctions: an update, Geological Society of America Special Papers, v. 505.

Bowring, S. A., & Schmitz, M. D., 2003, High-precision U-Pb zircon geochronology and the stratigraphic record, Reviews in Mineralogy and Geochemistry, v. 53, p. 305-326.

Corbett, M.J., and Watkins, D.K., 2013, Calcareous nannofossil paleoecology of the Mid-Cretaceous Western Interior Seaway and evidence of oligotrophic surface waters during OAE2, Palaeogeography, Palaeoclimatology, Palaeoecology, v. 392, p. 510-523.

Corbett, M.J., Watkins, D.K., and Pospichal, J.J., 2014, A qualitative analysis of calcareous nannofossil bioevents of the Late Cretaceous (Late Cenomanian-Coniacian) Western Interior Seaway and their reliability in established zonation schemes: Marine Micropaleontology v. 109, p. 30-45.

Dawson, W.C., 2000, Shale Microfacies: Eagle Ford Group (Cenomanian-Turonian) North-Central Texas Outcrops and Subsurface Equivalents, Gulf Coast Association of Geological Societies Transactions, v. 1.

Davis, D.W., Krogh, T.E., and Williams, I.S., 2003, Historical development of zircon geochronology, Reviews in mineralogy and geochemistry, v. 53, p. 145-181.

Denne, R.A., et al., 2014, The Cenomanian-Turonian Eagle Ford Group of South Texas: Insights on timing and paleoceanographic conditions from geochemistry and micropaleontologic analyses, Palaeogeography, Palaeoclimatology, Palaeoecology, v. 413, p. 2-28.

Donovan, A. D., and Staerker, T.S., 2010, Sequence stratigraphy of the Eagle Ford (Boquillas) Formation in the subsurface of South Texas and outcrops of West Texas, The Gulf Coast association of geological societies transactions, v. 60, p. 861-899.

Donovan, A. D., et al., 2012, The Eagle Ford outcrops of West Texas: A laboratory for under-standing heterogeneities within unconventional mudstone reservoirs, Gulf Coast Association of Geological Societies Journal, v. 1, p. 162–185.

Elder, W.P., 1988, Geometry of Upper Cretaceous bentonite beds: Implications about volcanic source areas and paleowind patterns, western interior, United States, Geology v. 16, p. 835-838.

Eldrett, J.S., Minisini, D., and Bergman, S.C., 2014, Decoupling of the carbon cycle during Ocean Anoxic Event 2, Geology, v. 42, p. 567-570.

Gardner, R.D., et al., 2013, Comparative Stratigraphy of the Eagle Ford Group Strata in Lozier Canyon and Antonio Creek, Terrell County, Texas, Gulf Coast Association of Geological Societies Journal, v. 2, p. 42-52.

Gradstein, F.M, Ogg, J.G., Schmitz, M.D., et al., 2012, The Geologic Time Scale 2012: Boston, USA, Elsevier, DOI: 10.1016/B978-0-444-59425-9.00004-4.

Hentz, T.F., and Ruppel, S.C., 2010, Regional Lithostratigraphy of the Eagle Ford Shale: Maverick Basin to East Texas Basin, Gulf Coast Association of Geological Societies Transactions, v.60, p. 325-337.

Hentz, T.F., Ambrose, W.A., and Smith, D.C., 2014, Eaglebine play of the southwestern East Texas Basin: Stratigraphic and depositional framework of the Upper Cretaceous (Cenomanian-Turonian) Woodbine and Eagle Ford Groups, AAPG Bulletin, v. 98, p. 2551-2580.

Jenkyns, H.C., 2010, Geochemistry of oceanic anoxic events, Geochemistry, Geophysics, Geosystems, v. 11.3.

Ludwig, K.R., 1991, ISOPLOT; a plotting and regression program for radiogenic-isotope data for Microsoft excel; version 2.53. No. 91-445. US Geological Survey.

Mattinson, J. M., 2005, Zircon U–Pb chemical abrasion ("CA-TIMS") method: combined annealing and multi-step partial dissolution analysis for improved precision and accuracy of zircon ages, Chemical Geology, v. 220, p. 47-66.

Ma et al., 2014., Testing the astronomical time scale for oceanic anoxic event 2, and its extension into Cenomanian strata of the Western Interior Basin (USA), GSA Bulletin v. 126, p. 974-989.

Meyers, S.R. (2014), astrochron: An R Package for Astrochronology. http://cran.r-project.org/package=astrochron (accessed June 2014).

Meyers, S.R., Hinnov, L.A., 2010, Northern Hemisphere glaciation and the evolution of Plio-Pleistocene climate noise, Paleoceanography, v. 25.

Meyers, S.R., et al., 2012, Intercalibration of radioisotopic and astrochronologic time scales for the Cenomanian-Turonian boundary interval, Western Interior Basin, USA:, Geology, v. 40, p. 7-10.

Raup, D.M., and Sepkoski, J.J., 1984, Periodicity of extinctions in the geologic past, PCNAS, v. 81, p. 801-805.

Samperton, K.M., et al., 2015, Magma emplacement, differentiation and cooling in the middle crust: integrated zircon geochronological–geochemical constraints from the Bergell Intrusion, Central Alps, Chemical Geology v. 417, p. 322–340.

Schlanger, S. O., Jenkyns, H.C., 2007, Cretaceous oceanic anoxic events: causes and consequences, Netherlands Journal of Geosciences/Geologie en Mijnbouw, Classic Papers.

Schmitz, M.D., and Bowring, S.A., 2001, The significance of U–Pb zircon dates in lower crustal xenoliths from the southwestern margin of the Kaapvaal craton, southern Africa, Chemical Geology , v. 172, p. 59-76.

Schoene, B., et al., 2006, Reassessing the uranium decay constants for geochronology using ID-TIMS U–Pb data, Geochimica et Cosmochimica Acta, v. 70, p. 426-445.

Sloss, L., 1963, Sequences of the cratonic interior of North America: Geological Society of America Bulletin, v. 74, p. 93–114.

Tian, Y., Ayers, W. B., and McCain, D., 2013, The Eagle Ford Shale Play, South Texas: Regional Variations in Fluid Types, Hydrocarbon Production and Reservoir Properties, IPTC 2013: International Petroleum Technology Conference, Beijing, China.

Turgeon, S.C., and Creaser, R.A., 2008, Cretaceous oceanic anoxic event 2 triggered by a massive magmatic episode, Nature, v. 454, p. 323-326.

Wetherill, G.W., 1956, Discordant uranium–lead ages: Transactions of the American Geophysical Union, v. 37, p. 320–326.

APPENDIX A

FIGURES

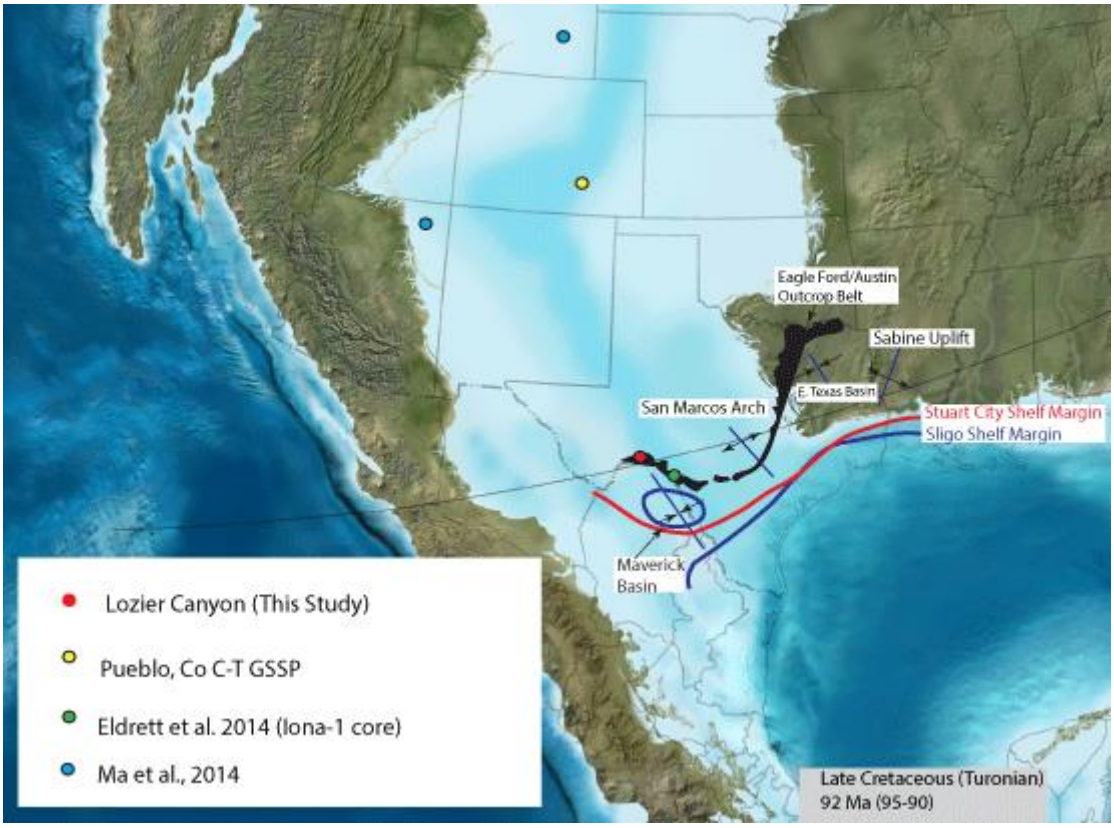

Figure 1. Paleogeographic reconstruction of the WIS during the Late Cretaceous. Previous study sites are indicated, as well as key components of the Eagle Ford. Modified from Blakey (2014) and Donovan et al. (2012).

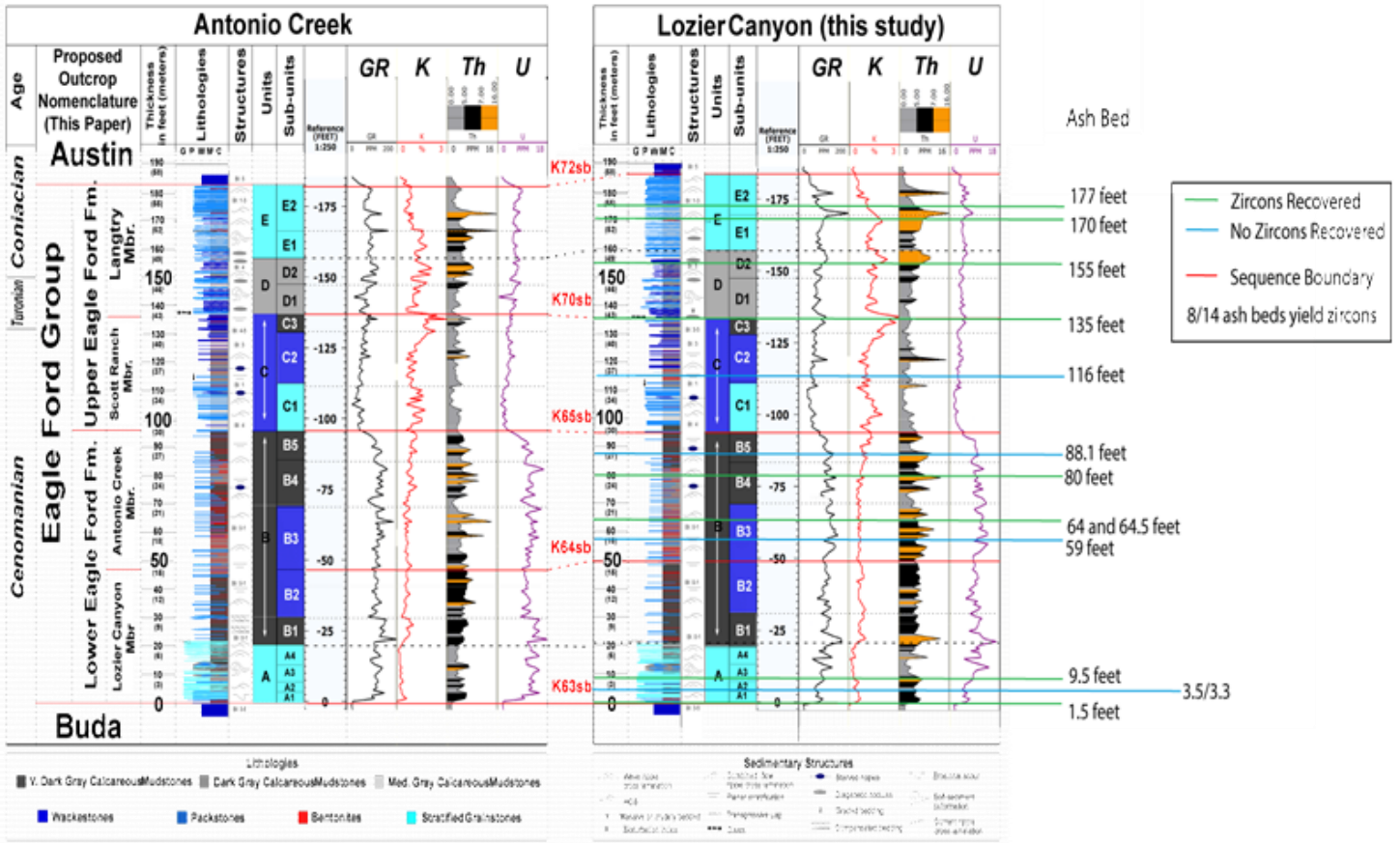

Figure 2. Lithology and spectral gamma ray log correlation of Lozier Canyon and Antonio Creek. modified from Gardner, 2013. Green lines denote ash beds that are zircon bearing. These ash beds were analyzed for ID-TIMS analysis, excluding 3.0, 3.5, 9.5, and 64. Modified after Gardner et al., 2013.

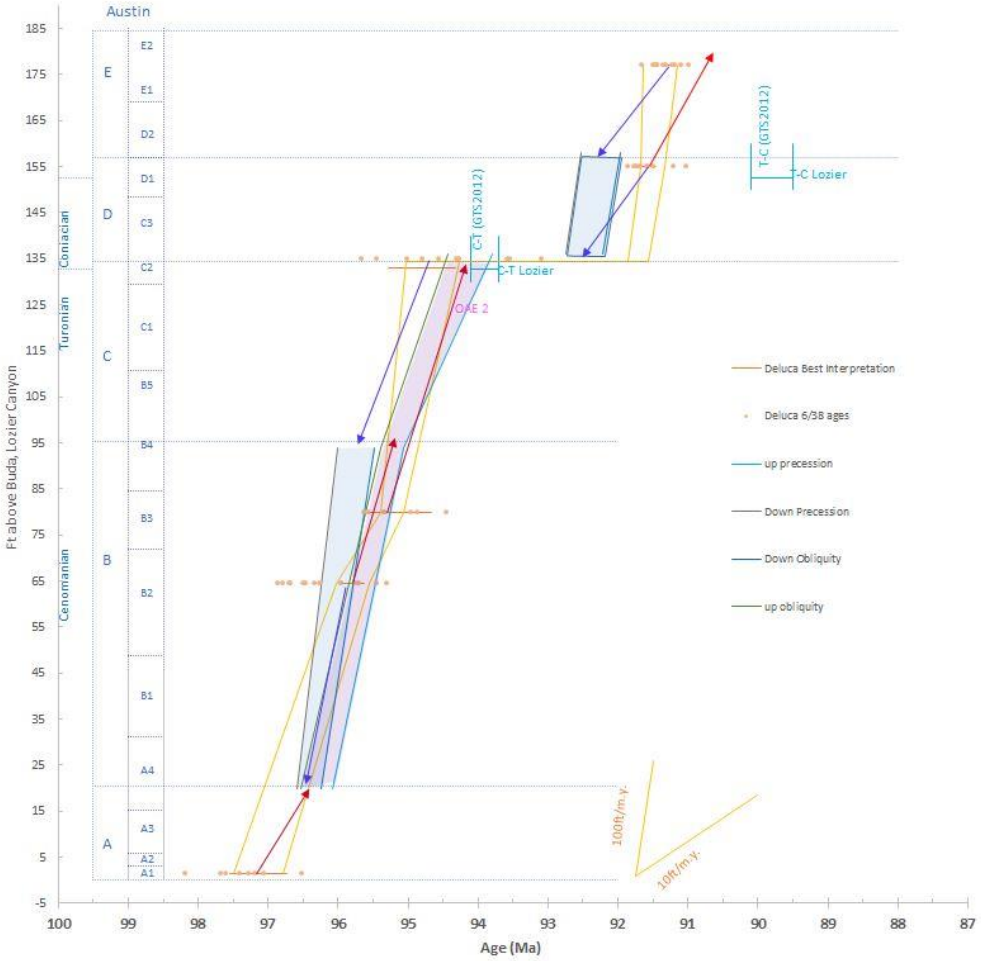

Figure 3. Cyclostratigraphic analysis of facies dataset. Red arrows denote bottom-up analyzed sections; blue arrows denote top-down analyzed sections. The purple polygon represents the possible range of sedimentation rates for bottom-up analyzed sections; the blue polygons represent the possible range of sedimentation rates for top-down analyzed sections. Note that all sections originate from a single dated ash bed, from which each analysis is anchored. All sections terminate at significant boundary markers. Facies values are from Gardner et al., 2013.

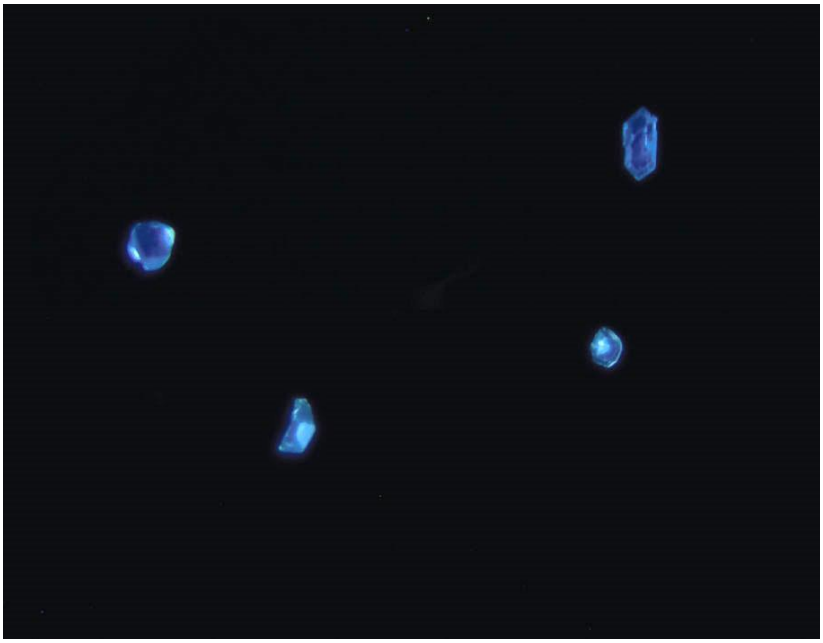

Figure 4. Cathodoluminescence images of zircons from sample 1.5. Zircons from sample 1.5 are characteristically dull under cathodoluminescence and typically show little to no zonation.

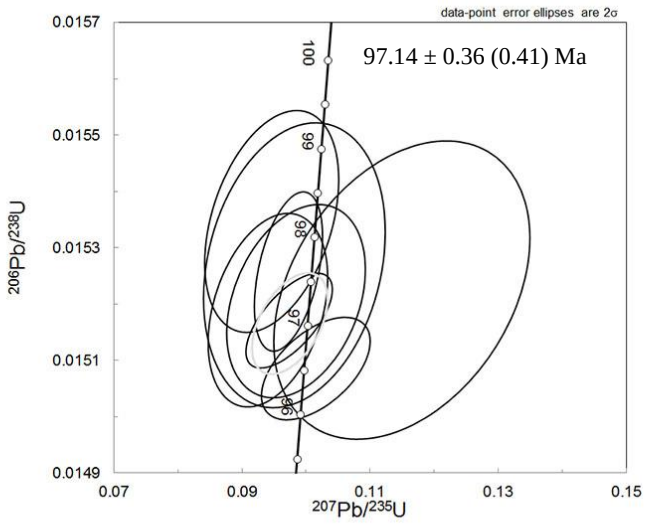

Figure 5. Concordia diagram for sample 1.5.

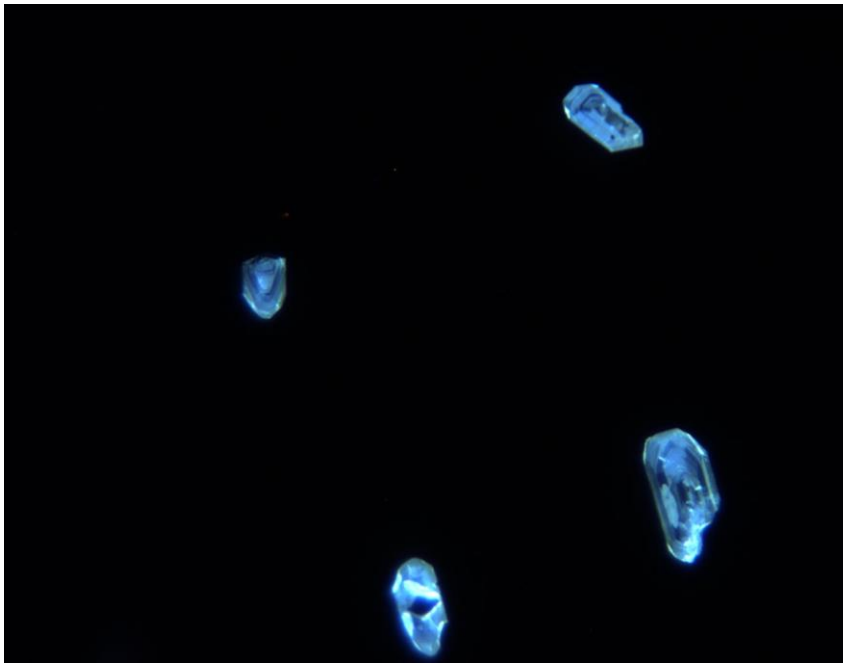

Figure 6. Cathodoluminescence images of zircons from sample 64.5. A large portion of zircons from sample 64.5 show complex internal zonation, and were excluded from analysis. Results from zircon analyses support evidence for inheritance of xenocrystic components into zircons within 64.5, which become apparent under CL imaging.

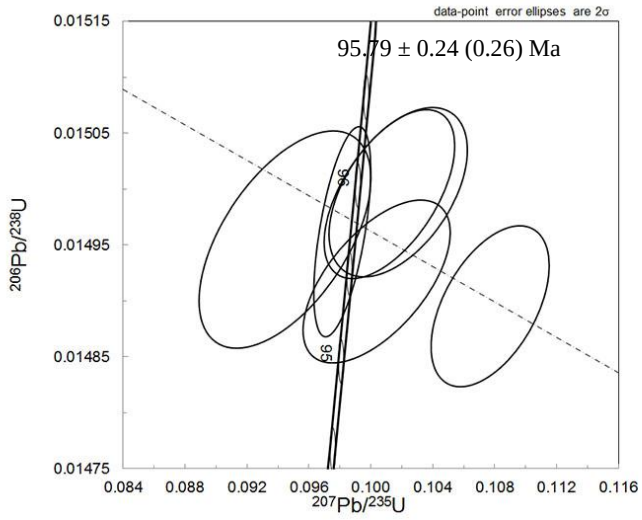

Figure 7. Concordia diagram for sample 64.5. Dashed line is the linear regression of analyses to account for variable Pb_o composition (see text for discussion).

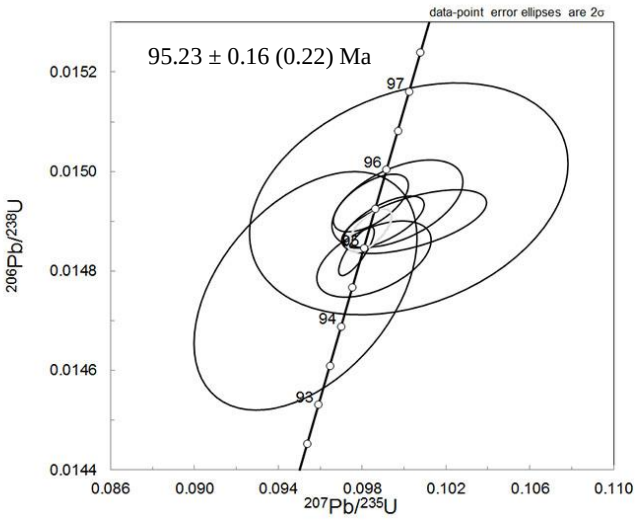

Figure 8. Concordia diagram for sample 80.

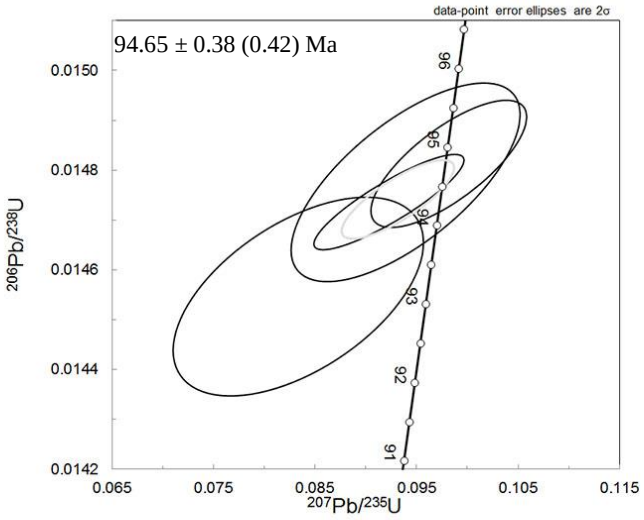

Figure 9. Concordia diagram for sample 135.

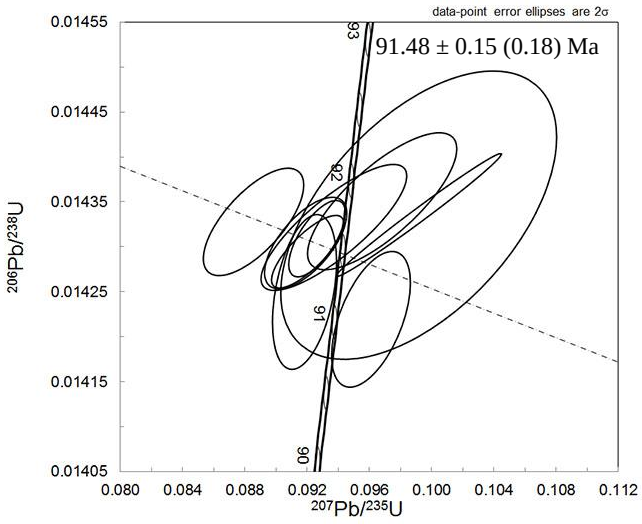

Figure 10. Concordia diagram for sample 155. Dashed line is the linear regression of analyses to account for variable Pb_o composition (see text for discussion).

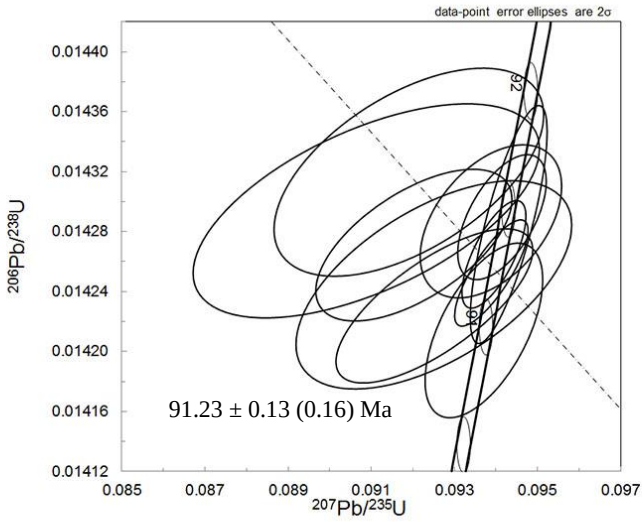

Figure 11. Concordia diagram for sample 177. Dashed line is the linear regression of analyses to account for variable Pb_o composition (see text for discussion).

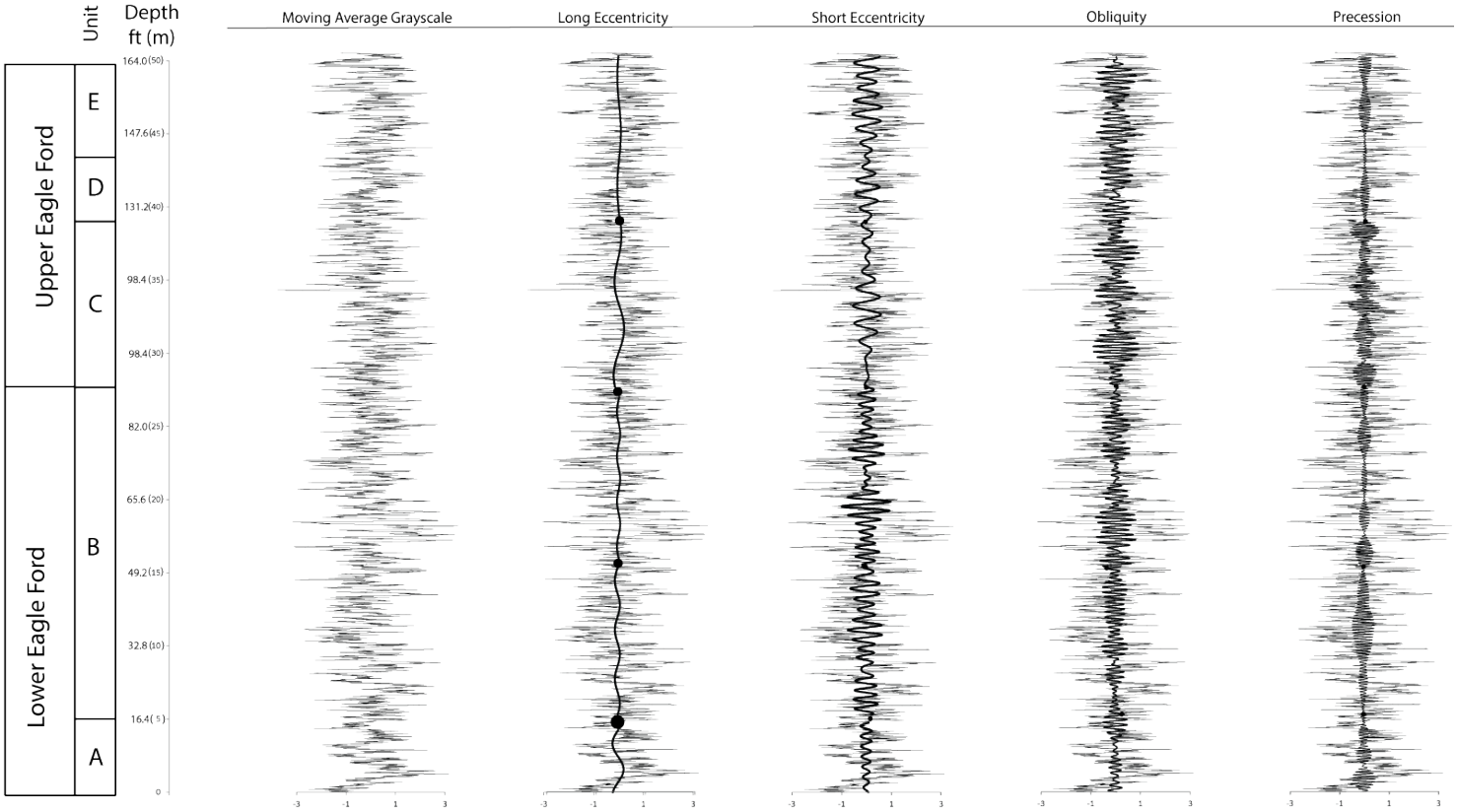

Figure 12. Band-pass filter results for the BP-Schlumberger Lozier Canyon #1 core. Filtering parameters are listed in table 4. All bandpass results are constructed from the moving average grayscale dataset (left). Black dots represent the junction of separately analyzed sections.

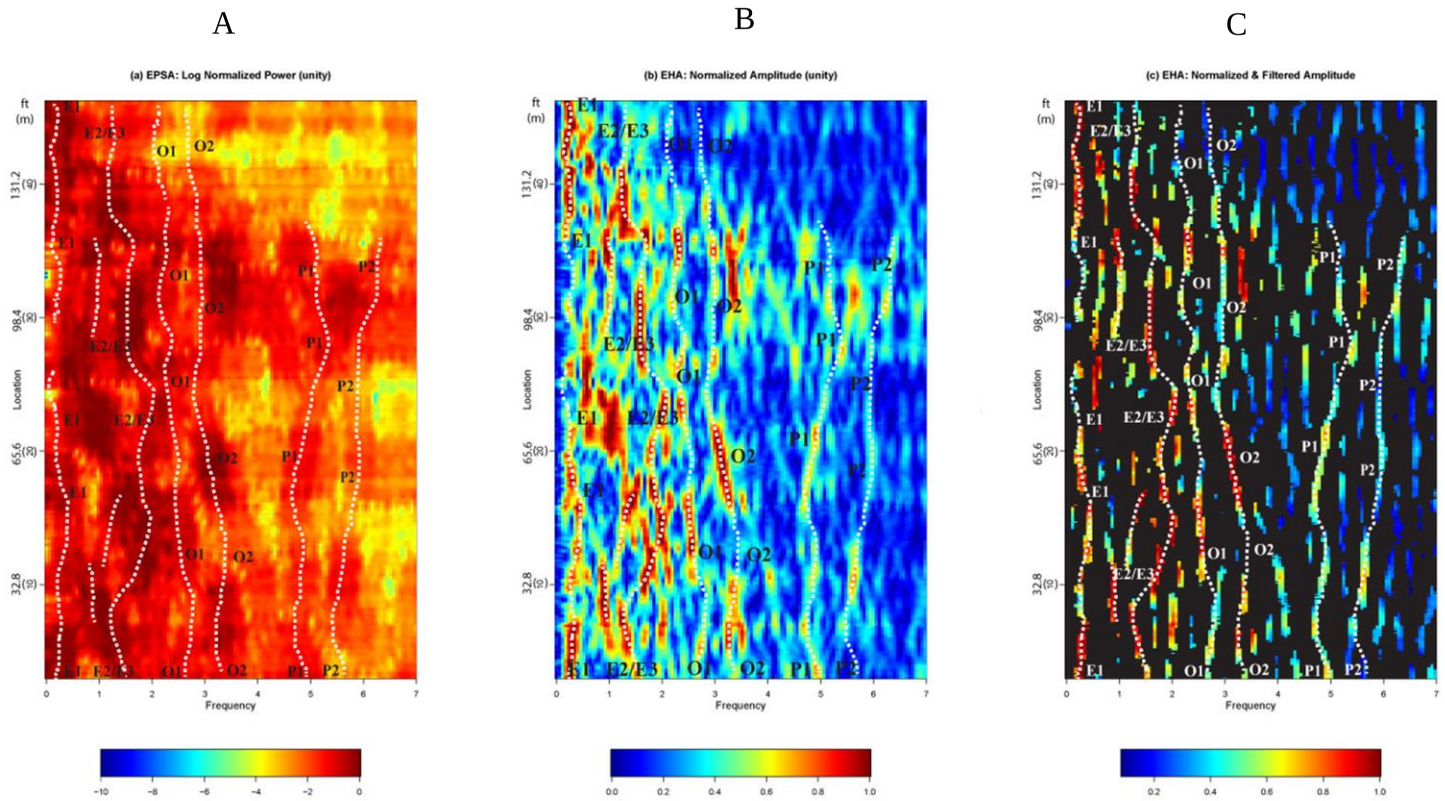

Figure 13. EHA and EPSA results for grayscale data from the Eagle Ford at Lozier Canyon. All analyses employ three 2π tapers and a 6 m moving window. A. Evolutive Power Spectral analysis results (log $_{10}$ power); B. Evolutive harmonic analysis amplitude results; C. Filtered EHA results (filtered at 80% confidence level). Orbital terms labelled: long eccentricity (E1), short eccentricity (E2, E3), obliquity (O1, O2), and precession (P1, P2).

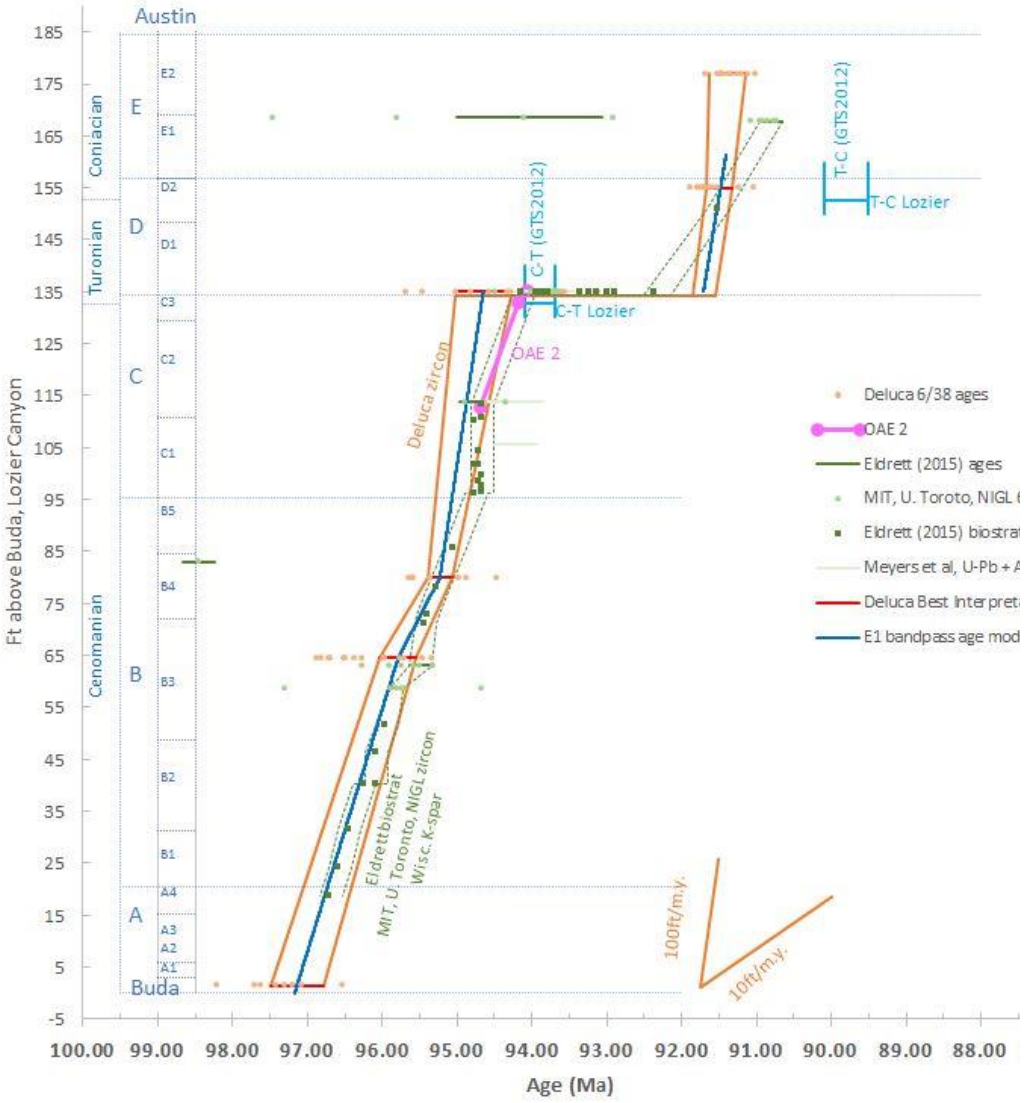

Figure 14. Lozier Canyon and WIS chronostratigraphic comparison. ID-TIMS zircon ages and E1 age model from Lozier Canyon. Supplemental biostratigraphic and geochronologic data from correlative WIS sections is included from Eldrett et al. (2015) and Meyers et al. (2012).

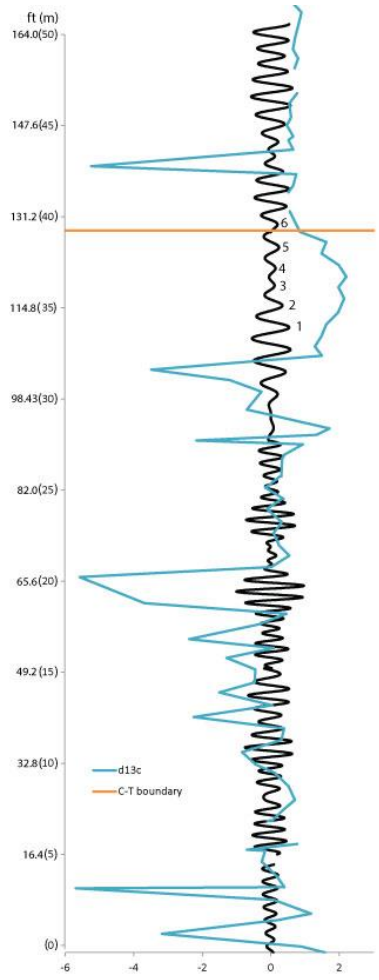

Figure 15 Short Eccentricity bandpass (black) and bulk $\delta^{13}C$ data (blue) for Lozier Canyon. Cycles 1-6 are counted peak to peak.

APPENDIX B

TABLES

Sample (ft)	Age (Ma)*	Interpretation Method Utilized	Location	Ash Bed Details
177	91.23 ± 0.13 (0.16)	Regression	Osman Canyon	Common zircons; scatter in ages associated with complex Pb_o composition
155	91.88 ± 0.15 (0.18)	Regression	Osman Canyon	Abundant zircons; scatter in ages associated with complex Pb_o composition
135	94.65 ± 0.38 (0.42)	Concordia age of youngest 4	Antonio Creek	Scarce zircons, multiple xenocrystic components; rare sanidine
80	95.23 ± 0.16 (0.22)	Concordia age	Antonio Creek	Uncommon zircons, minor xenocrystic component
64.5	95.79 ± 0.24 (0.26)	Regression of youngest 6 grains	Antonio Creek	Abundant zircons; rare sanidine; complex xenocrystic components and complex Pb_o composition scatter
1.5	97.14 ±.36 (.41)	Concordia age	Antonio Creek	Uncommon zircons; highly concordant

Table 1. Sampled ash bed summaries.
*reported as X±Y(Z), where X is age, Y is standard error without decay constant uncertainty, and Z is standard error with decay constant uncertainty.

	Compositional Parameters								Radiogenic Isotope Ratios									Isotopic Ages						
	U	Pb	Th	$^{206}Pb^*$	mol %	Pb*	Pb_c	^{206}Pb	^{208}Pb	^{207}Pb		^{207}Pb		^{206}Pb		corr.	^{207}Pb		^{207}Pb		^{206}Pb		
	pg	pg	U	x10^{-13} mol	$^{206}Pb^*$	Pb_c	(pg)	^{204}Pb	^{206}Pb	^{206}Pb	% err	^{235}U	% err	^{238}U	% err	coef.	^{206}Pb	±	^{235}U	±	^{238}U	±	
EF Lozier 1.5 (UTM: 29°49.571 N 101°37.431 W)																								
(Z5) EF Lozier 1-5	180.39	4.69	0.632	0.1134	0.8426	1.67	1.75	115.12	0.2058	0.04881	6.585	0.10153	6.835	0.015086	0.4929	0.5342	138.95	154.58	98.19	6.40	96.52	0.472
(Z7) EF Lozier 1-5	155.86	9.62	0.834	0.0989	0.5462	0.40	6.85	39.60	0.3028	0.05477	13.785	0.11497	14.215	0.015225	1.4218	0.3485	402.75	308.62	110.50	14.88	97.41	1.374
(Z27) EF Lozier 1-5	169.42	4.33	0.779	0.1071	0.8567	1.92	1.48	126.74	0.2422	0.04655	5.375	0.09737	5.663	0.015171	0.4533	0.6581	26.19	128.88	94.35	5.10	97.06	0.436
(Z26) Ef Lozier 1.5	75.79	2.36	0.501	0.0480	0.7715	1.02	1.17	79.79	0.1570	0.04696	8.729	0.09845	8.988	0.015205	0.9225	0.3284	47.09	208.45	95.34	8.18	97.28	0.890
(Z2) EF Lozier 1.5	88.21	3.25	1.104	0.0561	0.7386	0.98	1.64	69.38	0.3436	0.04664	11.567	0.09819	11.808	0.015269	1.3541	0.2337	30.91	277.10	95.11	10.72	97.69	1.312
(Z19) EF Lozier 1.5	155.54	3.42	0.709	0.0989	0.9064	3.09	0.84	196.14	0.2190	0.04623	4.195	0.09726	4.470	0.015258	0.7577	0.4376	9.78	100.88	94.25	4.02	97.62	0.733
(Z21) EF Lozier 1.5	85.34	3.10	0.842	0.0546	0.7339	0.89	1.64	68.17	0.2520	0.04473	8.697	0.09465	9.036	0.015347	1.0492	0.3744	-70.36	212.40	91.82	7.93	98.18	1.022
(Z43) EF Lozier 1.5	291.60	8.16	0.695	0.1846	0.8193	1.41	3.38	99.74	0.2089	0.04491	7.847	0.09405	8.110	0.015189	0.9248	0.3369	-60.60	191.27	91.27	7.08	97.18	0.891
(Concordia age used for age interpretation)																								
	Compositional Parameters								Radiogenic Isotope Ratios									Isotopic Ages						
	U	Pb	Th	$^{206}Pb^*$	mol %	Pb*	Pb_c	^{206}Pb	^{208}Pb	^{207}Pb		^{207}Pb		^{206}Pb		corr.	^{207}Pb		^{207}Pb		^{206}Pb		
	pg	pg	U	x10^{-13} mol	$^{206}Pb^*$	Pb_c	(pg)	^{204}Pb	^{206}Pb	^{206}Pb	% err	^{235}U	% err	^{238}U	% err	coef.	^{206}Pb	±	^{235}U	±	^{238}U	±	
EF Lozier 64.5 (UTM: 29°50.819 N 101°46.333 W)																								
(Z35) EF Lozier 64-5	338.77	6.74	0.398	0.2103	0.9168	3.27	1.58	218.08	0.1387	0.05244	2.718	0.10770	2.895	0.014895	0.3949	0.5034	304.73	61.91	103.86	2.86	95.31	0.373
(Z30) EF Lozier 64-5	318.65	6.60	0.363	0.1981	0.8996	2.60	1.83	180.38	0.1182	0.04880	3.646	0.10037	3.871	0.014917	0.3989	0.6004	138.24	85.59	97.12	3.59	95.45	0.378
(Z61) EF Lozier 64-5	219.57	6.36	0.395	0.1368	0.7877	1.07	3.06	84.93	0.1212	0.04580	4.524	0.09445	4.802	0.014955	0.5310	0.5630	-12.70	109.26	91.64	4.21	95.69	0.504
(Z41) EF Lozier 64.5	804.49	14.94	0.492	0.5016	0.9436	5.00	2.49	320.04	0.1562	0.04758	1.299	0.09815	1.530	0.014962	0.5132	0.5851	78.34	30.83	95.07	1.39	95.74	0.487
(Z28) EF Lozier 64-5	237.48	5.30	0.420	0.1484	0.8804	2.18	1.67	151.69	0.1370	0.04894	3.190	0.10120	3.406	0.014996	0.4116	0.5700	145.18	74.79	97.88	3.18	95.95	0.392
(Z33) EF Lozier 64-5	186.04	3.65	0.369	0.1163	0.9187	3.33	0.84	225.79	0.1212	0.04921	3.402	0.10177	3.588	0.014997	0.4126	0.4968	158.03	79.58	98.40	3.36	95.96	0.393
(Z40) EF Lozier 64.5	345.59	6.82	0.426	0.2166	0.9220	3.50	1.52	232.72	0.1378	0.04849	2.194	0.10058	2.482	0.015044	0.6331	0.5569	123.14	51.65	97.31	2.30	96.26	0.604
(Z31) EF Lozier 64-5	550.88	10.19	0.550	0.3456	0.9529	6.23	1.41	386.20	0.1816	0.04953	1.401	0.10283	1.557	0.015057	0.2412	0.6945	173.09	32.68	99.39	1.47	96.34	0.230
(Z2) EF Lozier 64.5	293.89	6.24	0.566	0.1846	0.9068	2.97	1.57	194.64	0.1783	0.04718	1.965	0.09808	2.160	0.015076	0.2873	0.7120	58.45	46.84	95.00	1.96	96.46	0.275
(Z1) EF Lozier 64.5	921.03	18.72	0.384	0.5788	0.9106	2.96	4.73	201.17	0.1237	0.04836	1.396	0.10057	1.589	0.015082	0.2677	0.7605	117.12	32.91	97.31	1.47	96.50	0.256
(Z3) EF Lozier 64.5	518.08	10.33	0.484	0.3262	0.9241	3.65	2.22	238.24	0.1562	0.04843	1.504	0.10090	1.681	0.015111	0.2721	0.6948	120.28	35.43	97.61	1.56	96.68	0.261
(Z4) EF Lozier 64.5	305.55	6.26	0.415	0.1924	0.9100	2.97	1.57	201.56	0.1320	0.04768	2.016	0.09935	2.216	0.015112	0.2731	0.7590	83.31	47.83	96.17	2.03	96.69	0.262
(Z51) EF Lozier 64.5	153.33	4.31	0.403	0.0966	0.8017	1.18	1.98	91.28	0.1228	0.04556	5.222	0.09503	5.498	0.015127	0.5195	0.5660	-25.49	126.43	92.18	4.85	96.79	0.499
(Z52) EF Lozier 64-5	279.10	6.14	0.494	0.1761	0.8910	2.44	1.78	166.19	0.1526	0.04618	2.220	0.09639	2.422	0.015140	0.3061	0.6960	6.84	53.43	93.44	2.16	96.86	0.294
(Regression of youngest 6 grains used for age interpretation)																								
	Compositional Parameters								Radiogenic Isotope Ratios									Isotopic Ages						
	U	Pb	Th	$^{206}Pb^*$	mol %	Pb*	Pb_c	^{206}Pb	^{208}Pb	^{207}Pb		^{207}Pb		^{206}Pb		corr.	^{207}Pb		^{207}Pb		^{206}Pb		
	pg	pg	U	x10^{-13} mol	$^{206}Pb^*$	Pb_c	(pg)	^{204}Pb	^{206}Pb	^{206}Pb	% err	^{235}U	% err	^{238}U	% err	coef.	^{206}Pb	±	^{235}U	±	^{238}U	±	
EF Lozier 80 (UTM:29°50.903 N 101°46.328 W)																								
(91) EF Lozier 80	125.10	3.54	0.760	0.0779	0.8157	1.43	1.45	98.57	0.2464	0.04864	5.933	0.10022	6.193	0.014945	1.2740	0.3023	130.36	139.51	96.98	5.73	95.63	1.208
(Z5) EF Lozier 80	846.75	13.81	0.464	0.5236	0.9796	14.48	0.89	900.56	0.1481	0.04776	0.518	0.09773	0.709	0.014840	0.2699	0.8026	87.52	12.28	94.68	0.64	94.96	0.254
(Z7) EF Lozier 80	150.72	3.01	0.438	0.0936	0.9150	3.24	0.71	216.93	0.1429	0.04891	2.619	0.10048	2.812	0.014899	0.3512	0.5925	143.53	61.43	97.22	2.61	95.34	0.332
(Z8) EF Lozier 80	605.96	10.87	0.517	0.3727	0.9512	5.88	1.58	372.03	0.1619	0.04683	4.149	0.09530	4.559	0.014760	1.3268	0.4410	40.37	99.20	92.43	4.03	94.45	1.243
(Z9) EF Lozier 80	226.96	4.50	0.634	0.1402	0.9292	4.14	0.88	259.14	0.2042	0.04822	2.084	0.09856	2.262	0.014824	0.4220	0.4991	110.18	49.18	95.45	2.06	94.86	0.397
(Z10) EF Lozier 80	314.35	5.77	0.552	0.1957	0.9508	5.96	0.83	373.39	0.1762	0.04779	1.317	0.09842	1.487	0.014937	0.3179	0.6111	88.72	31.20	95.31	1.35	95.58	0.301
(Z52) EF Lozier 80	347.46	6.70	0.584	0.2157	0.9370	4.61	1.19	289.44	0.1880	0.04821	1.410	0.09904	1.586	0.014898	0.2872	0.6707	109.68	33.27	95.89	1.45	95.33	0.272
(Z55) EF Lozier 80	293.43	6.04	0.626	0.1826	0.9191	3.55	1.33	224.83	0.2021	0.04841	2.357	0.09968	2.560	0.014935	0.4810	0.4994	119.16	55.54	96.48	2.36	95.57	0.456
(Concordia age used for age interpretation)																								
	Compositional Parameters								Radiogenic Isotope Ratios									Isotopic Ages						
	U	Pb	Th	$^{206}Pb^*$	mol %	Pb*	Pb_c	^{206}Pb	^{208}Pb	^{207}Pb		^{207}Pb		^{206}Pb		corr.	^{207}Pb		^{207}Pb		^{206}Pb		
	pg	pg	U	x10^{-13} mol	$^{206}Pb^*$	Pb_c	(pg)	^{204}Pb	^{206}Pb	^{206}Pb	% err	^{235}U	% err	^{238}U	% err	coef.	^{206}Pb	±	^{235}U	±	^{238}U	±	
EF Lozier 135 (UTM: 29°51.287 N 101°46.377 W)																								
(Z37) EF Lozier 135	186.06	4.06	0.643	0.1143	0.8925	2.57	1.14	162.24	0.1954	0.04542	6.089	0.09228	6.550	0.014736	0.5304	0.8780	-33.13	147.65	89.63	5.62	94.30	0.496
(Z38) EF Lozier 135	137.54	2.94	0.556	0.0834	0.8864	2.33	0.88	153.45	0.1553	0.04156	11.526	0.08335	12.095	0.014546	1.1200	0.5424	-253.33	291.71	81.29	9.45	93.10	1.034
(Z39) EF Lozier 135	195.59	4.52	0.800	0.1207	0.8872	2.56	1.27	154.56	0.2567	0.04807	5.887	0.09818	6.387	0.014813	0.7038	0.7389	102.70	139.13	95.09	5.80	94.79	0.662
(Z40) EF Lozier 135	173.59	4.41	0.663	0.1069	0.8429	1.67	1.65	110.96	0.2045	0.04610	9.099	0.09382	9.816	0.014776	1.1015	0.6837	3.02	219.10	91.15	8.56	94.55	1.033
(Z41) EF Lozier 135	116.55	2.28	0.725	0.0710	0.9326	4.38	0.42	258.72	0.2230	0.04596	5.755	0.09262	6.180	0.014618	1.1171	0.4579	-4.71	138.79	89.94	5.32	93.55	1.037
(Z42) EF Lozier 135	113.48	2.35	0.742	0.0691	0.9154	3.45	0.53	206.09	0.2313	0.04663	5.676	0.09401	6.086	0.014623	0.8299	0.5457	30.19	135.98	91.23	5.31	93.58	0.770
(Z43) EF Lozier 135	130.26	3.51	0.682	0.0800	0.8198	1.41	1.46	96.72	0.2016	0.04412	18.942	0.08961	19.789	0.014732	1.2197	0.7105	-104.15	465.60	87.14	16.53	94.28	1.141
(Z3) EF Lozier 135	171.34	3.60	0.776	0.1065	0.9241	3.98	0.72	229.79	0.2595	0.05019	4.391	0.10323	4.743	0.014916	0.4331	0.8263	203.87	101.87	99.75	4.51	95.44	0.410
(Z4) EF Lozier 135	69.43	1.86	0.884	0.0430	0.8353	1.66	0.70	105.84	0.2640	0.04461	13.676	0.09132	14.333	0.014847	0.8600	0.7762	-76.86	334.41	88.73	12.18	95.00	0.810
(Z11)EF Lozier 135	112.53	2.54	0.636	0.0701	0.8902	2.55	0.72	158.78	0.2119	0.04998	6.205	0.10302	6.662	0.014951	0.5136	0.8978	193.88	144.21	99.56	6.32	95.67	0.487
Concordia age of 4 youngest grains used for age interpretation																								
	Compositional Parameters								Radiogenic Isotope Ratios									Isotopic Ages						
	U	Pb	Th	$^{206}Pb^*$	mol %	Pb*	Pb_c	^{206}Pb	^{208}Pb	^{207}Pb		^{207}Pb		^{206}Pb		corr.	^{207}Pb		^{207}Pb		^{206}Pb		
	pg	pg	U	x10^{-13} mol	$^{206}Pb^*$	Pb_c	(pg)	^{204}Pb	^{206}Pb	^{206}Pb	% err	^{235}U	% err	^{238}U	% err	coef.	^{206}Pb	±	^{235}U	±	^{238}U	±	
EF Lozier 155 (UTM: 29°49.536 N 101°37.405 W)																								
(Z45) EF Lozier 155	341.22	5.48	0.260	0.2037	0.9566	6.17	0.76	401.68	0.0782	0.04483	2.753	0.08856	2.976	0.014328	0.3402	0.6859	-64.92	67.16	86.16	2.46	91.71	0.309
(Z46) EF Lozier 155	941.90	14.41	0.312	0.5616	0.9758	11.50	1.15	720.11	0.0980	0.04695	1.449	0.09264	1.602	0.014309	0.2426	0.6789	46.84	34.59	89.96	1.38	91.59	0.220
(Z47) EF Lozier 155	797.54	12.32	0.353	0.4750	0.9756	11.54	0.98	715.46	0.1103	0.04669	1.886	0.09203	2.061	0.014295	0.2308	0.7822	33.65	45.15	89.40	1.76	91.50	0.209
(Z48) EF Lozier 155	660.52	14.53	0.239	0.3941	0.8575	1.69	5.40	127.12	0.0759	0.04746	3.762	0.09372	4.081	0.014322	0.3996	0.8171	72.57	89.40	90.97	3.55	91.67	0.363
(Z49) EF Lozier 155	470.26	7.21	0.267	0.2803	0.9714	9.57	0.68	609.85	0.0835	0.04660	2.175	0.09191	2.352	0.014304	0.2907	0.6466	28.86	52.12	89.28	2.01	91.56	0.264
(Z50) EF Lozier 155	442.68	18.35	0.289	0.2644	0.6428	0.52	12.10	51.38	0.0968	0.05017	6.850	0.09917	7.301	0.014335	0.9135	0.5406	203.07	158.92	96.01	6.69	91.75	0.831
(Z3) EF Lozier 155	421.05	8.18	0.378	0.2515	0.9092	2.94	2.08	192.47	0.1268	0.05019	3.983	0.09920	4.369	0.014336	0.3897	0.9907	203.59	92.40	96.03	4.00	91.76	0.355
(Z5) EF Lozier 155	1381.97	22.56	0.320	0.8188	0.9565	6.33	3.08	408.96	0.1047	0.04902	1.955	0.09611	2.152	0.014220	0.4334	0.5350	148.76	45.80	93.18	1.92	91.02	0.391
(Z29) EF Lozier 155	524.81	9.86	0.314	0.3138	0.9150	3.09	2.41	207.32	0.1028	0.04893	3.726	0.09682	4.048	0.014351	0.4335	0.7649	144.66	87.38	93.84	3.63	91.85	0.395
(Z62) EF Lozier 155	1753.37	26.20	0.330	1.0410	0.9827	16.27	1.52	1007.58	0.1033	0.04674	1.699	0.09183	1.829	0.014250	0.4933	0.3893	35.99	40.66	89.21	1.56	91.21	0.446
*Regression age used for age interpretation																								
	Compositional Parameters								Radiogenic Isotope Ratios									Isotopic Ages						
	U	Pb	Th	$^{206}Pb^*$	mol %	Pb*	Pb_c	^{206}Pb	^{208}Pb	^{207}Pb		^{207}Pb		^{206}Pb		corr.	^{207}Pb		^{207}Pb		^{206}Pb		
	pg	pg	U	x10^{-13} mol	$^{206}Pb^*$	Pb_c	(pg)	^{204}Pb	^{206}Pb	^{206}Pb	% err	^{235}U	% err	^{238}U	% err	coef.	^{206}Pb	±	^{235}U	±	^{238}U	±	
EF Lozier 177 (UTM: 29°49.571 N 101°37.431 W)																								
(Z14) EF Lozier 177	1054.02	17.35	0.517	0.6275	0.9692	9.50	1.65	588.01	0.1648	0.04766	1.372	0.09388	1.481	0.014287	0.2920	0.4570	82.29	32.55	91.11	1.29	91.45	0.265
(Z16) EF Lozier 177	317.71	5.68	0.486	0.1889	0.9390	4.63	1.01	299.46	0.1522	0.04677	1.934	0.09202	2.095	0.014271	0.2897	0.6034	37.40	46.28	89.39	1.79	91.35	0.263
(Z18) EF Lozier 177	1555.96	23.76	0.506	0.9248	0.9910	33.78	0.68	2057.09	0.1617	0.04777	0.544	0.09395	0.669	0.014265	0.2056	0.7051	87.76	12.89	91.18	0.58	91.31	0.186
(Z37) EF Lozier 177	1153.97	18.04	0.532	0.6871	0.9864	22.29	0.77	1352.99	0.1701	0.04778	0.811	0.09414	0.924	0.014290	0.2384	0.5741	88.54	19.22	91.36	0.81	91.47	0.216
(Z38) EF Lozier 177	393.41	7.84	0.572	0.2343	0.9096	3.06	1.93	200.24	0.1768	0.04611	3.525	0.09088	3.747	0.014294	0.4082	0.5819	3.48	84.87	88.32	3.17	91.49	0.370
(Z17) EF Lozier 177	1329.22	22.36	0.791	0.7913	0.9833	19.17	1.11	1090.38	0.2532	0.04788	0.529	0.09431	0.801	0.014285	0.4543	0.7798	93.41	12.53	91.51	0.70	91.43	0.412
(Z32) EF Lozier 177	691.32	11.41	0.644	0.4106	0.9771	13.46	0.79	801.09	0.2057	0.04778	0.618	0.09389	0.768	0.014252	0.2031	0.8008	88.25	14.64	91.12	0.67	91.23	0.184
(Z29) EF Lozier 177	523.80	8.58	0.552	0.3102	0.9716	10.57	0.74	648.09	0.1767	0.04781	1.076	0.09371	1.234	0.014214	0.3348	0.5788	90.10	25.49	90.95	1.07	90.98	0.302
(Z86) EF Lozier 177	353.69	7.18	0.709	0.2099	0.9121	3.29	1.67	206.34	0.2235	0.04710	2.721	0.09251	2.930	0.014244	0.3984	0.5733	54.29	64.90	89.83	2.52	91.18	0.360
(Z20) EF Lozier 177	174.10	3.54	0.586	0.1039	0.9042	2.92	0.90	191.363	0.1826	0.04655	2.687	0.09190	2.884	0.014320	0.3959	0.5503	26.09	64.41	89.28	2.46	91.66	0.360
(Z23) EF Lozier 177	567.87	10.79	0.538	0.3367	0.9228	3.62	2.34	234.227	0.1699	0.04715	1.888	0.09252	2.091	0.014230	0.2951	0.7244	56.96	45.01	89.85	1.80	91.09	0.267
*Regression age used for age interpretation																								

Table 2. Zircon ID-TIMS Analyses utilized for final age interpretation.

Lozier Interval	Ash bed age interpolated sedimentation rate
155-177	1.635 cm/kyr
135-155	n/d; unconformity
80-135	1.32 cm/kyr
64.5 to 80	0.7 cm/kyr
1.5 to 64.5	1.48 cm/kyr

Table 3. Sedimentation rates derived by linear interpolation of time between dated ash beds.

Top down sections (ft)	Obliquity (ft/ka)	Precession (ft/ka)	Median ft/ka	Median cm/ka
177-158	0.0996	0.0564	0.0780	2.38
155-136	0.0490	0.0302	0.0396	1.21
135-94	0.0254	0.0150	0.0202	0.62
64.5-20	0.0256	0.0146	0.0201	0.61

Table 4. Rock accumulation rates derived from cyclostratigraphic facies analysis of Lozier Canyon from top to bottom. Approximate median value presented in figure 3 as red arrows.

Bottom up sections (ft)	Obliquity (ft/ka)	Precession (ft/ka)	Median ft/ka	Median cm/ka
155-180	0.0272	0.0152	0.0212	0.65
80-135	0.0683	0.0390	0.0537	1.64
64.5-94	0.0730	0.0405	0.0568	1.73
1.5-20	0.0334	0.0188	0.0261	0.80

Table 5. Rock accumulation rates derived from cyclostratigraphic facies analysis of Lozier Canyon from bottom to top. Approximate median value presented in figure 3 as blue arrows.

Interval (ft)	Rock Accumulation Rate (cm/ka)
124.67-160.76	0.866
88.58-124.67	0.876
49.21-88.58	0.652
17.028-49.21	0.794
0-17.028	0.599

Table 6. Rock accumulation rates derived from ASM testing.

	E1	E2/E3	O1/O2	P1/P2
38-49m	0.1-.16	0.9-1.3	2.1-3.1	5.5-5.9
27-38m	0.1-.2	0.7-.99	2.2-3	5.1-6.31
15-27m	0.3-.35	1.2-1.9	2.3-3.2	5.4-6.0
5.18-15m	0.3-.35	1.1-1.8	2.5-3.31	4.9-5.61
0-5.18m	0.1-.31	1.4-1.6	2.6-3.36	4.9-5.8

Table 7. Bandpass parameters used for analyses derived from ASM analyses. These parameters were applied as bandpass filters to the Eagle Ford Grayscale dataset to isolate long eccentricity, short eccentricity, obliquity, and precession signals.

APPENDIX C

SUPPLEMENTAL OBSERVATIONS

Additional ash bed lithologies

Ash bed 9.5 is ~3 inches thick, densely lithified, and dark gray to brown with surficial oxidation. Mineralogy consists of abundant zircons, apatites, Fe oxides, quartz, clays, and calcite. SEM microprobe analysis suggests the dominant clay species is kaolinite. Zircons are 2-20 microns in size (C-axis) and are sub-rounded to prismatic with rare inclusions, and range in color from clear to pale yellow. Several zircons were analyzed for ash bed 9.5, however offer only preliminary age estimates and were not assigned an age interpretation.

Ash bed 170 is 2 inches thick, well-lithified, beige to yellow with abundant clays, calcite, and Fe oxides. Zircons are abundant and are sub-rounded to prismatic, and range in size from 10-20 microns. Grains are generally clear and free of inclusions. Several zircons were analyzed for ash bed 9.5, however offer only preliminary age estimates and were not assigned an age interpretation.

APPENDIX D

SUPPLEMENTAL TABLES

Term	Mean LA04/LA11 frequency (cycle/ka)	Nδ	Corresponding Laskar04/Laskar11 period (ka)	2δ uncertainty (cycles/ka)	% Uncertainty in frequency
E1	2.485000×10^{-3}	4	402.41	0	0%
E2	0.007918×10^{-3}	8	126.29	2.006000×10^{-3}	7.83%
E3	1.046300×10^{-2}	8	95.58	4.900000×10^{-4}	4.68%
O1	2.007414×10^{-2}	7	49.82	2.133824×10^{-3}	1.06%
O2	2.657542×10^{-2}	7	37.63	4.850230×10^{-4}	1.83%
P1	4.442543×10^{-2}	7	22.51	7.936403×10^{-3}	1.79%
P2	5.446250×10^{-2}	7	18.36	8.446071×10^{-3}	1.55%

Table S1. Target periods used in ASM analyses for the Upper Eagle Ford, based on Eldrett et al., 2015 and the time domain of 91-94.5 Ma astronomical model of Laskar et al., 2004, 2001.

Term	Mean LA04/LA11 frequency (cycle/ka)	Nδ	Corresponding Laskar04/Laskar11 period (ka)	2δ uncertainty (cycles/ka)	% Uncertainty in frequency
E1	2.468133×10^{-3}	4	405.16	2.164530×10^{-5}	0.87%
E2	7.852000×10^{-3}	8	127.35	2.420000×10^{-4}	3.08%
E3	1.033200×10^{-2}	8	96.78	2.310000×10^{-4}	2.23%
O1	1.991018×10^{-2}	8	50.23	1.427431×10^{-3}	7.17%
O2	2.654691×10^{-2}	8	37.67	5.645561×10^{-4}	2.13%
P1	4.478543×10^{-2}	8	22.33	1.943272×10^{-3}	4.34%
P2	5.436627×10^{-2}	8	18.39	$1.107492 \times 10^{-}$	2.04%

Table S2. Target periods used in ASM analyses for the Lower Eagle Ford, based on Eldrett et al., 2015 and the time domain of 94-98 Ma astronomical model of Laskar et al., 2004, 2001.

0-5.18m

Observed frequency cycles/m	MTM harmonic Probability (%)	Observed Period (ka)	Resolution bandwidth (ka)	Laskar04/Laskar11 target period (ka) (Eldrett et al., 2015)
0.3086	99.05	540.15	227.32-852.98	E1:405.17
1.5046	97.28	110.80	46.63-174.97	E2:127.38 E3:96.79
2.7006	93.04	61.73	25.98-97.48	O1:50.29
3.3565	98.92	49.67	20.90-78.44	O2:37.67
4.9769	99.52	33.50	14.10-52.90	P1:22.34
5.7870	95.23	28.81	12.12-45.49	P2:18.4

Table S3. ASM- derived astronomical periods for the interval of 0-5.18 m in the Lower Eagle Ford using astronomical targets derived by Laskar et al. 2004, 2011, Eldrett et al., 2015.

5-15m

Observed frequency cycles/m	MTM harmonic Probability (%)	Observed Period (ka)	Resolution bandwidth (ka)	Laskar04/Laskar11 target period (ka) (Eldrett et al., 2015)
0.3259	88.43	386.60	268.47-504.74	E1:405.17
1.2017	94.91	104.84	72.80-136.88	E2:127.38
1.7313	90.68	72.77	50.53-95.01	E3:96.79
2.5257	96.41	49.88	34.64-65.13	O1:50.29
3.2997	92.70	38.18	26.52-49.85	O2:37.67
4.9292	90.56	25.56	17.75-33.37	P1:22.34
5.6013	96.53	22.49	15.62-29.37	P2:18.4

Table S4. ASM- derived astronomical periods for the interval of 5.18-15m in the Lower Eagle Ford using astronomical targets derived by Laskar et al. 2004, 2011, Eldrett et al., 2015.

15-27m

Observed frequency cycles/m	MTM harmonic Probability (%)	Observed Period (ka)	Resolution bandwidth (ka)	Laskar04/Laskar11 target period (ka) (Eldrett et al., 2015)
0.3167	80.07	484.040	363.06-605.02	E1:405.17
1.3000	85.93	117.907	88.44-147.38	E2:127.38
1.8000	89.73	85.155	63.87-106.44	E3:96.79
2.3500	99.06	65.225	48.92-81.53	O1:50.29
3.1167	95.13	49.180	36.89-61.47	O2:37.67
5.6667	93.85	27.049	20.29-33.80	P1:22.34
5.9333	99.82	25.834	19.38-32.29	P2:18.4

Table S5. ASM- derived astronomical periods for the interval of 15-27 m in the Lower Eagle Ford using astronomical targets derived by Laskar et al. 2004,2011, Eldrett et al., 2015.

27-38m

Observed frequency cycles/m	MTM harmonic Probability (%)	Observed Period (ka)	Resolution bandwidth (ka)	Laskar04/Laskar11 target period (ka) (Eldrett et al., 2015)
0.6179	97.30	184.73	134.37-235.10	E2:126.71
0.9814	99.58	116.31	84.60-148.03	E3:95.75
2.2535	95.27	36.84	36.84-64.46	O1:49.82
2.9441	99.66	28.20	28.20-49.34	O2:37.63
5.1613	98.55	16.09	16.09-28.15	P1:22.51
6.2880	95.51	13.20	13.20-23.10	P2:18.36

Table S6. ASM- derived astronomical periods for the interval of 27-38 m in the Lower Eagle Ford using astronomical targets derived by Laskar et al. 2004,2011, Eldrett et al., 2015.

38-49m

Observed frequency cycles/m	MTM harmonic Probability (%)	Observed Period (ka)	Resolution bandwidth (ka)	Laskar04/Laskar11 target period (ka) (Eldrett et al., 2015)
0.1455	96.69	784.40	570.53-998.26	E1:402.41
0.9641	99.75	118.40	86.12-150.68	E2:126.71
1.2915	95.68	88.38	64.29-112.48	E3:95.75
2.1101	97.41	54.10	39.35-68.85	O1:49.82
3.0196	99.74	37.80	27.50-48.11	O2:37.63
5.5117	94.74	20.71	15.06-26.36	P1:22.51
5.8755	99.50	19.43	14.13-24.72	P2:18.36

Table S7. ASM- derived astronomical periods for the interval of 38-49m in the Lower Eagle Ford using astronomical targets derived by Laskar et al. 2004,2011, Eldrett et al., 2015.

	Compositional Parameters								Radiogenic Isotope Ratios								Isotopic Ages					
	U	Pb	Th/U	$^{206}Pb^*$ x10^{13} mol	mol % $^{206}Pb^*$	Pb^*/Pb_c	Pb_c (pg)	$^{206}Pb/^{204}Pb$	$^{208}Pb/^{206}Pb$	$^{207}Pb/^{206}Pb$	% err	$^{207}Pb/^{235}U$	% err	$^{206}Pb/^{238}U$	% err	corr. coef.	$^{207}Pb/^{206}Pb$	±	$^{207}Pb/^{235}U$	±	$^{206}Pb/^{238}U$	±
	pg	pg																				
EF Lozier 1.5 (UTM: 29°49.571 N 101°37.431 W)																						
(Z5) EF Lozier 1-5	180.39	4.69	0.632	0.1134	0.8426	1.67	1.75	115.12	0.2058	0.04881	6.585	0.10153	6.835	0.015086	0.4929	0.5342	138.95	154.58	98.19	6.40	96.52	0.472
(Z7) EF Lozier 1-5	155.86	9.62	0.834	0.0989	0.5462	0.40	6.85	39.60	0.3028	0.05477	13.785	0.11497	14.215	0.015225	1.4218	0.3485	402.75	308.62	110.50	14.88	97.41	1.374
(Z27) EF Lozier 1-5	169.42	4.33	0.779	0.1071	0.8567	1.92	1.48	126.74	0.2422	0.04655	5.375	0.09737	5.663	0.015171	0.4533	0.6581	26.19	128.88	94.35	5.10	97.06	0.436
(Z26) Ef Lozier 1.5	75.79	2.36	0.501	0.0480	0.7715	1.02	1.17	79.79	0.1570	0.04696	8.729	0.09845	8.988	0.015205	0.9225	0.3284	47.09	208.45	95.34	8.18	97.28	0.890
(Z2) EF Lozier 1.5	88.21	3.25	1.104	0.0561	0.7386	0.98	1.64	69.38	0.3436	0.04664	11.567	0.09819	11.808	0.015269	1.3541	0.2337	30.91	277.10	95.11	10.72	97.69	1.312
(Z19) EF Lozier 1.5	155.54	3.42	0.709	0.0989	0.9064	3.09	0.84	196.14	0.2190	0.04623	4.195	0.09726	4.470	0.015258	0.7577	0.4376	9.78	100.88	94.25	4.02	97.62	0.733
(Z21) EF Lozier 1.5	85.34	3.10	0.842	0.0546	0.7339	0.89	1.64	68.17	0.2520	0.04473	8.697	0.09465	9.036	0.015347	1.0492	0.3744	-70.36	212.40	91.82	7.93	98.18	1.022
(Z43) EF Lozier 1.5	291.60	8.16	0.695	0.1846	0.8193	1.41	3.38	99.74	0.2089	0.04491	7.847	0.09405	8.110	0.015189	0.9248	0.3369	-60.60	191.27	91.27	7.08	97.18	0.891
(Z6) EF Lozier 1.5*	87.74	2.49	0.656	0.0545	0.8116	1.40	1.04	96.97	0.2371	0.05449	13.361	0.11193	13.523	0.014899	0.6297	0.2791	391.22	299.72	107.73	13.82	95.34	0.595
(Z9) EF Lozier 1.5*	111.64	3.01	0.564	0.0694	0.8217	1.42	1.24	102.13	0.1859	0.04945	8.744	0.10168	8.964	0.014913	0.5638	0.4167	169.14	204.13	98.32	8.40	95.43	0.534
(Z20) EF Lozier 1.5*	211.90	4.57	0.315	0.1399	0.9085	2.94	1.16	199.37	0.1221	0.05888	1.963	0.12863	2.158	0.015845	0.3334	0.6362	562.52	42.75	122.87	2.50	101.34	0.335
(Z22) EF Lozier 1.5*	59.52	1.92	0.508	0.0366	0.7327	0.74	1.10	68.28	0.0654	0.01877	70.070	0.03823	70.326	0.014771	2.0325	0.1402	-2923.83	3305.71	38.10	26.30	94.52	1.905
(Z44) EF Lozier 1.5*	137.01	15.6	0.658	0.0879	0.3547	0.17	13.35	27.80	0.2153	0.04911	41.046	0.10425	41.656	0.015397	3.7896	0.2051	153.04	961.10	100.70	39.93	98.50	3.701
(Z59) EF Lozier 1.5*	87.02	3.56	0.690	0.0573	0.6950	0.71	2.09	59.32	0.2051	0.04449	86.216	0.09698	86.512	0.015812	3.2316	0.1102	-83.74	2110.94	93.99	77.66	101.13	3.240
(Z61) EF Lozier 1.5*	81.81	3.46	0.721	0.0489	0.6416	0.53	2.27	50.44	0.1505	0.03074	42.470	0.06084	43.410	0.014356	6.9762	0.2136	-1084.98	1282.36	59.97	25.28	91.89	6.359
* concordia age used for age interpretation																						
EF Lozier 64.5 (UTM: 29°50.819 N 101°46.333 W)																						
(Z3) EF Lozier 64.5	518.08	10.33	0.484	0.3262	0.9241	3.65	2.22	238.24	0.1562	0.04843	1.504	0.10090	1.681	0.015111	0.2721	0.6948	120.28	35.43	97.61	1.56	96.68	0.261
(Z1) EF Lozier 64.5	921.03	18.72	0.384	0.5788	0.9106	2.96	4.73	201.17	0.1237	0.04836	1.396	0.10057	1.589	0.015082	0.2677	0.7605	117.12	32.91	97.31	1.47	96.50	0.256
(Z2) EF Lozier 64.5	293.89	6.24	0.566	0.1846	0.9068	2.97	1.57	194.64	0.1783	0.04718	1.965	0.09808	2.160	0.015076	0.2873	0.7120	58.45	46.84	95.00	1.96	96.46	0.275
(Z4) EF Lozier 64.5	305.55	6.26	0.415	0.1924	0.9100	2.97	1.57	201.56	0.1320	0.04768	2.016	0.09935	2.216	0.015112	0.2731	0.7590	83.31	47.83	96.17	2.03	96.69	0.262
(Z51) EF Lozier 64.5	153.33	4.31	0.403	0.0966	0.8017	1.18	1.98	91.28	0.1228	0.04556	5.222	0.09503	5.498	0.015127	0.5195	0.5660	-25.49	126.43	92.18	4.85	96.79	0.499
(Z52) EF Lozier 64-5	279.10	6.14	0.494	0.1761	0.8910	2.44	1.78	166.19	0.1526	0.04618	2.220	0.09639	2.422	0.015140	0.3061	0.6960	6.84	53.43	93.44	2.16	96.86	0.294
(Z28) EF Lozier 64-5	237.48	5.30	0.420	0.1484	0.8804	2.18	1.67	151.69	0.1370	0.04894	3.190	0.10120	3.406	0.014996	0.4116	0.5700	145.18	74.79	97.88	3.18	95.95	0.392
(Z30) EF Lozier 64-5	318.65	6.60	0.363	0.1981	0.8996	2.60	1.83	180.38	0.1182	0.04880	3.646	0.10037	3.871	0.014917	0.3989	0.6004	138.24	85.59	97.12	3.59	95.45	0.378
(Z31) EF Lozier 64-5	550.88	10.19	0.550	0.3456	0.9529	6.23	1.41	386.20	0.1816	0.04953	1.401	0.10283	1.557	0.015057	0.2412	0.6945	173.09	32.68	99.39	1.47	96.34	0.230
(Z33) EF Lozier 64-5	186.04	3.65	0.369	0.1163	0.9187	3.33	0.84	225.79	0.1212	0.04921	3.402	0.10177	3.588	0.014997	0.4126	0.4968	158.03	79.58	98.40	3.36	95.96	0.393
(Z35) EF Lozier 64-5	338.77	6.74	0.398	0.2103	0.9168	3.27	1.58	218.08	0.1387	0.05244	2.718	0.10770	2.895	0.014895	0.3949	0.5034	304.73	61.91	103.86	2.86	95.31	0.373
(Z61) EF Lozier 64-5	219.57	6.36	0.395	0.1368	0.7877	1.07	3.06	84.93	0.1212	0.04580	4.524	0.09445	4.802	0.014955	0.5310	0.5630	-12.70	109.26	91.64	4.21	95.69	0.504
(Z41) EF Lozier 64.5	804.49	14.94	0.492	0.5016	0.9436	5.00	2.49	320.04	0.1562	0.04758	1.299	0.09815	1.530	0.014962	0.5132	0.5851	78.34	30.83	95.07	1.39	95.74	0.487
(Z40) EF Lozier 64.5	345.59	6.82	0.426	0.2166	0.9220	3.50	1.52	232.72	0.1378	0.04849	2.194	0.10058	2.482	0.015044	0.6331	0.5569	123.14	51.65	97.31	2.30	96.26	0.604
(Z53) EF Lozier 64.5*	165.20	6.83	0.401	0.1049	0.6712	0.60	4.28	54.75	0.1305	0.04889	8.572	0.10272	8.897	0.015239	0.8625	0.4180	142.54	201.10	99.29	8.42	97.50	0.834
(Z27) EF Lozier 64.5*	265.16	4.77	0.442	0.1637	0.9418	4.77	0.83	315.76	0.1260	0.04247	3.697	0.08675	3.992	0.014815	0.7994	0.4559	-198.86	92.56	84.47	3.24	94.81	0.752
(Z81) EF Lozier 64.5*	374.38	7.31	0.440	0.2326	0.9226	3.53	1.61	234.39	0.1393	0.04740	3.085	0.09745	3.258	0.014911	0.5371	0.3952	69.31	73.37	94.42	2.94	95.41	0.508
(Z34) EF Lozier 64.5*	1007.18	16.40	0.370	0.6258	0.9761	11.98	1.26	762.09	0.1228	0.04982	0.712	0.10242	0.864	0.014911	0.2451	0.7053	186.52	16.58	99.01	0.81	95.41	0.232
(Z48) EF Lozier 64.5*	861.74	19.46	0.468	0.5311	0.8678	1.89	6.74	135.92	0.1223	0.03882	4.112	0.07916	4.356	0.014791	0.4057	0.6315	-429.08	107.82	77.36	3.24	94.65	0.381
(Z37) EF Lozier 64.5 (2 grains)*	60.51	2.03	0.436	0.0382	0.7409	0.85	1.10	70.44	0.1369	0.04699	15.762	0.09813	16.067	0.015144	1.2672	0.2778	48.91	376.27	95.05	14.58	96.89	1.218
(Z80) EF Lozier 64.5*	102.87	4.02	0.530	0.0630	0.6761	0.60	2.51	55.76	0.1263	0.03531	19.676	0.07161	20.028	0.014709	1.3322	0.2950	-684.16	544.20	70.23	13.59	94.13	1.244
(Z82) EF Lozier 64.5*	155.25	6.40	0.412	0.0981	0.6698	0.59	4.02	54.53	0.1291	0.04688	14.270	0.09805	14.694	0.015170	1.6558	0.3087	42.98	341.04	94.98	13.32	97.06	1.594
(Z42) EF Lozier 64.5*	729.06	13.08	0.437	0.4463	0.9352	4.09	2.57	278.58	0.1063	0.03598	5.096	0.07290	5.355	0.014693	0.7350	0.4126	-632.07	139.39	71.45	3.69	94.03	0.685
*Discordia of youngest 6 grains used for age interpretation																						
EF Lozier 80 (UTM:29°50.903 N 101°46.328 W)																						
(91) EF Lozier 80	125.10	3.54	0.760	0.0779	0.8157	1.43	1.45	98.57	0.2464	0.04864	5.933	0.10022	6.193	0.014945	1.2740	0.3023	130.36	139.51	96.98	5.73	95.63	1.208
(Z5) EF Lozier 80	846.75	13.81	0.464	0.5236	0.9796	14.5	0.89	900.56	0.1481	0.04776	0.518	0.09773	0.709	0.014840	0.2699	0.8026	87.52	12.28	94.68	0.64	94.96	0.254
(Z7) EF Lozier 80	150.72	3.01	0.438	0.0936	0.9150	3.24	0.71	216.93	0.1429	0.04891	2.619	0.10048	2.812	0.014899	0.3512	0.5925	143.53	61.43	97.22	2.61	95.34	0.332
(Z8) EF Lozier 80	605.96	10.87	0.517	0.3727	0.9512	5.88	1.58	372.03	0.1619	0.04683	4.149	0.09530	4.559	0.014760	1.3268	0.4410	40.37	99.20	92.43	4.03	94.45	1.243
(Z9) EF Lozier 80	226.96	4.50	0.634	0.1402	0.9292	4.14	0.88	259.14	0.2042	0.04822	2.084	0.09856	2.262	0.014824	0.4220	0.4991	110.18	49.18	95.45	2.06	94.86	0.397
(Z10) EF Lozier 80	314.35	5.77	0.552	0.1957	0.9508	5.96	0.83	373.39	0.1762	0.04779	1.317	0.09842	1.487	0.014937	0.3179	0.6111	88.72	31.20	95.31	1.35	95.58	0.301
(Z52) EF Lozier 80	347.46	6.70	0.584	0.2157	0.9370	4.61	1.19	289.44	0.1880	0.04821	1.410	0.09904	1.586	0.014898	0.2872	0.6707	109.68	33.27	95.89	1.45	95.33	0.272
(Z55) EF Lozier 80	293.43	6.04	0.626	0.1826	0.9191	3.55	1.33	224.83	0.2021	0.04841	2.357	0.09968	2.560	0.014935	0.4810	0.4994	119.16	55.54	96.48	2.36	95.57	0.456
(014) EF Lozier 80*	95.73	3.71	0.573	0.0590	0.6895	0.68	2.20	58.24	0.1894	0.04956	9.194	0.10116	9.758	0.014802	2.4836	0.3478	174.63	214.43	97.85	9.10	94.72	2.333
(Z6) EF Lozier 80*	469.26	9.33	0.503	0.2837	0.9120	3.11	2.27	205.33	0.1591	0.04732	2.188	0.09467	3.439	0.014510	2.5070	0.7726	65.45	52.08	91.84	3.02	92.86	2.309
(Z56) EF Lozier 80*	656.85	17.47	0.578	0.4132	0.8326	1.52	6.92	107.31	0.1885	0.04890	2.926	0.10178	4.128	0.015095	2.7227	0.7068	143.16	68.64	98.42	3.87	96.58	2.608
(Z57) EF Lozier 80*	232.52	5.08	0.553	0.1460	0.8945	2.58	1.42	172.26	0.1703	0.04603	2.146	0.09560	2.376	0.015063	0.4015	0.6314	-0.93	51.71	92.70	2.11	96.38	0.384
(Z58) EF Lozier 80*	296.69	6.73	0.812	0.1894	0.9054	3.11	1.64	191.73	0.2565	0.04735	2.869	0.10001	3.038	0.015317	0.3090	0.5826	67.11	68.27	96.78	2.80	97.99	0.300
*Concorida age used for age interpretation																						
EF Lozier 135 (UTM: 29°51.287 N 101°46.377 W)																						
(Z37) EF Lozier 135	186.06	4.06	0.643	0.1143	0.8925	2.57	1.14	162.24	0.1954	0.04542	6.089	0.09228	6.550	0.014736	0.5304	0.8780	-33.13	147.65	89.63	5.62	94.30	0.496
(Z38) EF Lozier 135	137.54	2.94	0.556	0.0834	0.8864	2.33	0.88	153.45	0.1553	0.04156	11.526	0.08335	12.095	0.014546	1.1200	0.5424	-253.33	291.71	81.29	9.45	93.10	1.034
(Z39) EF Lozier 135	195.59	4.52	0.800	0.1207	0.8872	2.56	1.27	154.56	0.2567	0.04807	5.887	0.09818	6.387	0.014813	0.7038	0.7389	102.70	139.13	95.09	5.80	94.79	0.662
(Z40) EF Lozier 135	173.59	4.41	0.663	0.1069	0.8429	1.67	1.65	110.96	0.2045	0.04610	9.099	0.09392	9.816	0.014776	1.1015	0.6837	3.02	219.10	91.15	8.56	94.55	1.033
(Z41) EF Lozier 135	116.55	2.28	0.725	0.0710	0.9326	4.38	0.42	258.72	0.2230	0.04596	5.755	0.09262	6.180	0.014618	1.1171	0.4579	-4.71	138.79	89.94	5.32	93.55	1.037
(Z42) EF Lozier 135	113.48	2.35	0.742	0.0691	0.9154	3.45	0.53	206.09	0.2313	0.04663	5.676	0.09401	6.086	0.014623	0.8299	0.5457	30.19	135.98	91.23	5.31	93.58	0.770
(Z43) EF Lozier 135	130.26	3.51	0.682	0.0800	0.8198	1.41	1.46	96.72	0.2016	0.04412	18.942	0.08961	19.789	0.014732	1.2197	0.7105	-104.15	465.60	87.14	16.53	94.28	1.141
(Z3) EF Lozier 135	171.34	3.60	0.776	0.1065	0.9241	3.98	0.72	229.79	0.2595	0.05019	4.391	0.10323	4.743	0.014916	0.4331	0.8263	203.87	101.87	99.75	4.51	95.44	0.410
(Z4) EF Lozier 135	69.43	1.86	0.884	0.0430	0.8353	1.66	0.70	105.84	0.2640	0.04461	13.676	0.09132	14.333	0.014847	0.8600	0.7762	-76.86	334.41	88.73	12.18	95.00	0.810
(Z11)EF Lozier 135	112.53	2.54	0.636	0.0701	0.8902	2.55	0.72	158.78	0.2119	0.04998	6.205	0.10302	6.662	0.014951	0.5136	0.8978	193.88	144.21	99.56	6.32	95.67	0.487
(Z55) EF Lozier 135*	793.16	28.31	0.687	0.4733	0.7123	0.80	15.74	63.95	0.2360	0.05151	5.092	0.10171	5.441	0.014319	0.7356	0.5272	263.89	116.83	98.35	5.10	91.65	0.669
(Z2) EF Lozier 135*	60.10	2.84	0.588	0.0382	0.6356	0.57	1.81	47.84	0.2416	0.06242	32.469	0.13135	33.735	0.015262	2.1117	0.6196	688.53	692.53	125.31	39.77	97.64	2.045
(Z12) EF Lozier 135*	67.27	2.31	0.649	0.0426	0.7497	0.96	1.18	69.65	0.2314	0.05375	19.295	0.11255	20.203	0.015189	1.3715	0.6805	360.39	435.21	108.30	20.75	97.18	1.322
Concorida age of 4 youngest grains used for age interpretation																						
EF Lozier 155 (UTM: 29°49.536 N 101°37.405 W)																						
(Z45) EF Lozier 155	341.22	5.48	0.260	0.2037	0.9566	6.17	0.76	401.68	0.0782	0.04483	2.753	0.08856	2.976	0.014328	0.3402	0.6859	-64.92	67.16	86.16	2.46	91.71	0.309
(Z46) EF Lozier 155	941.90	14.41	0.312	0.5616	0.9758	11.50	1.15	720.11	0.0980	0.04695	1.449	0.09264	1.602	0.014309	0.2426	0.6789	46.84	34.59	89.96	1.38	91.59	0.220
(Z47) EF Lozier 155	797.54	12.32	0.353	0.4750	0.9756	11.54	0.98	715.46	0.1103	0.04669	1.886	0.09203	2.061	0.014295	0.2308	0.7822	33.65	45.15	89.40	1.76	91.50	0.209
(Z48) EF Lozier 155	660.52	14.53	0.239	0.3941	0.8575	1.69	5.40	127.12	0.0759	0.04746	3.762	0.09372	4.081	0.014322	0.3996	0.8171	72.57	89.40	90.97	3.55	91.67	0.363
(Z49) EF Lozier 155	470.26	7.21	0.267	0.2803	0.9714	9.57	0.68	609.85	0.0835	0.04660	2.175	0.09191	2.352	0.014304	0.2907	0.6466	28.86	52.12	89.28	2.01	91.56	0.264
(Z50) EF Lozier 155	442.68	18.35	0.289	0.2644	0.6428	0.52	12.10	51.38	0.0968	0.05017	6.850	0.09917	7.301	0.014335	0.9135	0.5406	203.07	158.92	96.01	6.69	91.75	0.831
(Z3) EF Lozier 155	421.05	8.18	0.378	0.2515	0.9092	2.94	2.08	192.47	0.1268	0.05019	3.983	0.09920	4.369	0.014336	0.3897	0.9907	203.59	92.40	96.03	4.00	91.76	0.355
(Z5) EF Lozier 155	1381.97	22.56	0.320	0.8188	0.9565	6.33	3.08	408.96	0.1047	0.04902	1.955	0.09611	2.152	0.014220	0.4334	0.5350	148.76	45.80	93.18	1.92	91.02	0.391
(Z29) EF Lozier 155	524.81	9.86	0.314	0.3138	0.9150	3.09	2.41	207.32	0.1028	0.04893	3.726	0.09682	4.048	0.014351	0.4335	0.7649	144.66	87.38	93.84	3.63	91.85	0.395
(Z62) EF Lozier 155	1753.37	26.20	0.330	1.0410	0.9827	16.27	1.52	1007.58	0.1033	0.04674	1.699	0.09183	1.829	0.014250	0.4933	0.3893	35.99	40.66	89.21	1.56	91.21	0.446
(Z44) EF Lozier 155*	447.24	7.11	0.296	0.2735	0.9718	9.82	0.66	617.92	0.0958	0.04844	1.665	0.09800	1.839	0.014675	0.2629	0.7001	120.63	39.22	94.93	1.67	93.91	0.245
(Z63) EF Lozier 155*	2551.63	47.03	0.476	1.8320	0.9893	27.62	1.64	1626.24	0.1527	0.04836	0.573	0.11487	0.777	0.017228	0.3606	0.7240	116.72	13.50	110.41	0.81	110.11	0.393
*Discordia age used for age interpretation																						
EF Lozier 177(UTM: 29°49.571 N 101°37.431 W)																						
(Z14) EF Lozier 177	1054.02	17.35	0.517	0.6275	0.9692	9.50	1.65	588.01	0.1648	0.04766	1.372	0.09388	1.481	0.014287	0.2920	0.4570	82.29	32.55	91.11	1.29	91.45	0.265
(Z16) EF Lozier 177	317.71	5.68	0.486	0.1889	0.9390	4.63	1.01	299.46	0.1522	0.04677	1.934	0.09202	2.095	0.014271	0.2897	0.6034	37.40	46.28	89.39	1.79	91.35	0.263
(Z18) EF Lozier 177	1555.96	23.76	0.506	0.9248	0.9910	33.78	0.68	2057.09	0.1617	0.04777	0.544	0.09395	0.669	0.014265	0.2056	0.7051	87.76	12.89	91.18	0.58	91.31	0.186
(Z37) EF Lozier 177	1153.97	18.04	0.532	0.6871	0.9864	22.29	0.77	1352.99	0.1701	0.04778	0.811	0.09414	0.924	0.014290	0.2384	0.5741	88.54	19.22	91.36	0.81	91.47	0.216
(Z38) EF Lozier 177	393.41	7.84	0.572	0.2343	0.9096	3.06	1.93	200.24	0.1768	0.04611	3.525	0.09088	3.747	0.014294	0.4082	0.5819	3.48	84.87	88.32	3.17	91.49	0.370
(Z17) EF Lozier 177	1329.22	22.36	0.791	0.7913	0.9833	19.17	1.11	1090.38	0.2532	0.04788	0.529	0.09431	0.801	0.014285	0.4543	0.7798	93.41	12.53	91.51	0.70	91.43	0.412
(Z32) EF Lozier 177	691.32	11.41	0.644	0.4106	0.9771	13.46	0.79	801.09	0.2057	0.04778	0.618	0.09389	0.768	0.014252	0.2031	0.8008	88.25	14.64	91.12	0.67	91.23	0.184
(Z29) EF Lozier 177	523.80	8.58	0.552	0.3102	0.9716	10.57	0.74	648.09	0.1767	0.04781	1.076	0.09371	1.234	0.014214	0.3348	0.5788	90.10	25.49	90.95	1.07	90.98	0.302
(Z86) EF Lozier 177	353.69	7.18	0.709	0.2099	0.9121	3.29	1.67	206.34	0.2235	0.04710	2.721	0.09251	2.930	0.014244	0.3984	0.5733	54.29	64.90	89.83	2.52	91.18	0.360
(Z20) EF Lozier 177	174.10	3.54	0.586	0.1039	0.9042	2.92	0.90	191.363	0.1826	0.04655	2.687	0.09190	2.884	0.014320	0.3959	0.5503	26.09	64.41	89.28	2.46	91.66	0.36
(Z23) EF Lozier 177	567.87	10.79	0.538	0.3367	0.9228	3.62	2.34	234.227	0.1699	0.04715	1.888	0.09252	2.091	0.014230	0.2951	0.7244	56.96	45.01	89.85	1.80	91.09	0.267
(Z15) EF Lozier 177*	1536.13	21.90	0.090	0.9172	0.9799	13.08	1.56	902.61	0.0287	0.04778	1.212	0.09441	3.032	0.014333	2.8306	0.9169	88.20	28.71	91.61	2.66	91.74	2.575
(Z30) EF Lozier 177*	992.14	21.43	1.462	0.6079	0.9591	8.97	2.15	442.05	0.4851	0.04976	0.809	0.10086	0.986	0.014699	0.2667	0.7397	183.91	18.85	97.57	0.92	94.07	0.249
(Z31) EF Lozier 177*	1039.08	20.12	0.739	0.6582	0.9592	7.66	2.32	442.66	0.2574	0.05241	2.337	0.10982	2.529	0.015199	0.4581	0.4938	303.17	53.24	105.80	2.54	97.24	0.442
(Z84) Ef Lozier 177 *	429.97	7.51	0.555	0.2519	0.9425	4.93	1.27	316.56	0.1595	0.04277	3.502	0.08290	3.818	0.014058	0.9996	0.4336	-181.05	87.38	80.87	2.97	89.99	0.892
(Z87) Ef Lozier 177 *	256.18	5.28	0.480	0.1510	0.8835	2.21	1.65	155.71	0.1284	0.03970	4.216	0.07742	4.545	0.014143	0.9832	0.4307	-370.42	109.24	75.71	3.32	90.53	0.883
(Z88) Ef Lozier 177 *	230.13	4.69	0.631	0.1351	0.8939	2.54	1.32	171.50	0.1671	0.03931	3.578	0.07637	5.004	0.014092	3.2869	0.7004	-396.25	93.21	74.73	3.61	90.21	2.942
(Z85) EF Lozier 177*	243.78	4.84	0.511	0.1445	0.9040	2.83	1.26	189.68	0.1543	0.04499	2.679	0.08822	3.060	0.014222	1.0443	0.5130	-56.25	65.23	85.84	2.52	91.03	0.943
*Discordia age used for age interpretation																						

Table S8. All ID-TIMS U/Pb analyses, including those discarded for final age interpretation.